



HAL
open science

A multidisciplinary study of a syntectonic pluton close to a major lithospheric-scale fault: relationships between the Montmarault granitic massif and the Sillon Houiller Fault in the Variscan French Massif Central. Part I: Geochronology, mineral fabrics and tectonic implications

Aurore Joly, Yan Chen, Michel Faure, Guillaume Martelet

► **To cite this version:**

Aurore Joly, Yan Chen, Michel Faure, Guillaume Martelet. A multidisciplinary study of a syntectonic pluton close to a major lithospheric-scale fault: relationships between the Montmarault granitic massif and the Sillon Houiller Fault in the Variscan French Massif Central. Part I: Geochronology, mineral fabrics and tectonic implications. *Journal of Geophysical Research*, 2007, 112 (B10104), pp.1-18. 10.1029/2006JB004745 . insu-00170187

HAL Id: insu-00170187

<https://insu.hal.science/insu-00170187>

Submitted on 2 Nov 2010

HAL is a multi-disciplinary open access archive for the deposit and dissemination of scientific research documents, whether they are published or not. The documents may come from teaching and research institutions in France or abroad, or from public or private research centers.

L'archive ouverte pluridisciplinaire **HAL**, est destinée au dépôt et à la diffusion de documents scientifiques de niveau recherche, publiés ou non, émanant des établissements d'enseignement et de recherche français ou étrangers, des laboratoires publics ou privés.



A multidisciplinary study of a syntectonic pluton close to a major lithospheric-scale fault—Relationships between the Montmarault granitic massif and the Sillon Houiller Fault in the Variscan French Massif Central:

1. Geochronology, mineral fabrics, and tectonic implications

Aurore Joly,^{1,2} Yan Chen,¹ Michel Faure,¹ and Guillaume Martelet²

Received 12 September 2006; revised 21 May 2007; accepted 2 August 2007; published 30 October 2007.

[1] Because of its location along one of the major faults, the Sillon Houiller Fault (SHF) of the French Massif Central (FMC), the Montmarault granitic pluton is well suited to better understand the place of the late orogenic magmatism in Variscan orogeny. Through a methodological approach, the close spatial association of the pluton with the lithospheric SHF is investigated in order to clarify the relationships between faulting and magmatic processes during the Late Carboniferous. Therefore a multidisciplinary study has been carried out on the Montmarault massif. Combining geochronology, field and laboratory microstructural observations, and anisotropy of magnetic susceptibility (AMS) methods presented in this paper and gravity and aeromagnetic modeling (part 2), as well as similar studies from other plutons in the FMC, allows us to draw the following conclusions: (1) The Montmarault pluton, dated by the chemical U-Th-Pb method on monazite at 321 ± 2 Ma, was emplaced in a NW-SE maximum stretching trend which is consistent with the regional extensional tectonic regime; (2) the Montmarault pluton is rooted in its eastern part along the SHF with a laccolite-like shape in its western part; (3) at circa 320 Ma, the “Proto-SHF” acted probably as a normal fault considered as the feeding channel for the magma emplacement; and (4) Late Carboniferous NE-SW extensional tectonics reworked the Montmarault pluton in a brittle postsolidus stage.

Citation: Joly, A., Y. Chen, M. Faure, and G. Martelet (2007), A multidisciplinary study of a syntectonic pluton close to a major lithospheric-scale fault—Relationships between the Montmarault granitic massif and the Sillon Houiller Fault in the Variscan French Massif Central: 1. Geochronology, mineral fabrics, and tectonic implications, *J. Geophys. Res.*, *112*, B10104, doi:10.1029/2006JB004745.

1. Introduction

[2] The Variscan French Massif Central (FMC) provides a good example of a complete orogenic cycle. The poly-phase tectonic, metamorphic and magmatic events are well documented. After the ductile and synmetamorphic nappe stacking events that took place from Late Silurian to Early Carboniferous times (from 420 to 340 Ma), numerous Middle to Late Carboniferous granitic plutons intruded the metamorphic basement (for details, see *Ledru et al.* [1989], *Faure* [1995], and *Faure et al.* [2005, and references therein]). The study of pluton architecture, emplacement mechanisms and tectonic settings are important to under-

stand the evolution of the continental crust after the collision. In the FMC, the plutons that have been studied extensively are essentially located in the western and southeastern parts of the FMC, namely, in the Limousin and Cévennes areas [e.g., *Mollier and Bouchez*, 1982; *Jover*, 1986; *Dumas et al.*, 1990; *Faure and Pons*, 1991; *Faure*, 1989, 1995; *Talbot et al.*, 2004, 2005; *Gébelin et al.*, 2004; *Be Mezème et al.*, 2006b] (Figure 1). The granitic plutons that crop out along one of the major faults of the FMC [e.g., *Grolier and Letourneur*, 1968], named the Sillon Houiller Fault (SHF), are poorly investigated. Along the SHF, a single Late Stephanian sinistral strike-slip offset has been only described so far. The pre-Stephanian activity of the SHF has not been well documented [*Feybesse*, 1981]. Therefore investigations with innovative and multidisciplinary methods of the plutons close to the SHF to determine the geometry of granitic bodies and their emplacement mechanisms might provide constraints to assess the regional tectonic style during the pluton em-

¹Institut des Sciences de la Terre d'Orléans, UMR CNRS 6113, Université d'Orléans, Orléans, France.

²Bureau de Recherches Géologiques et Minières, Orléans, France.

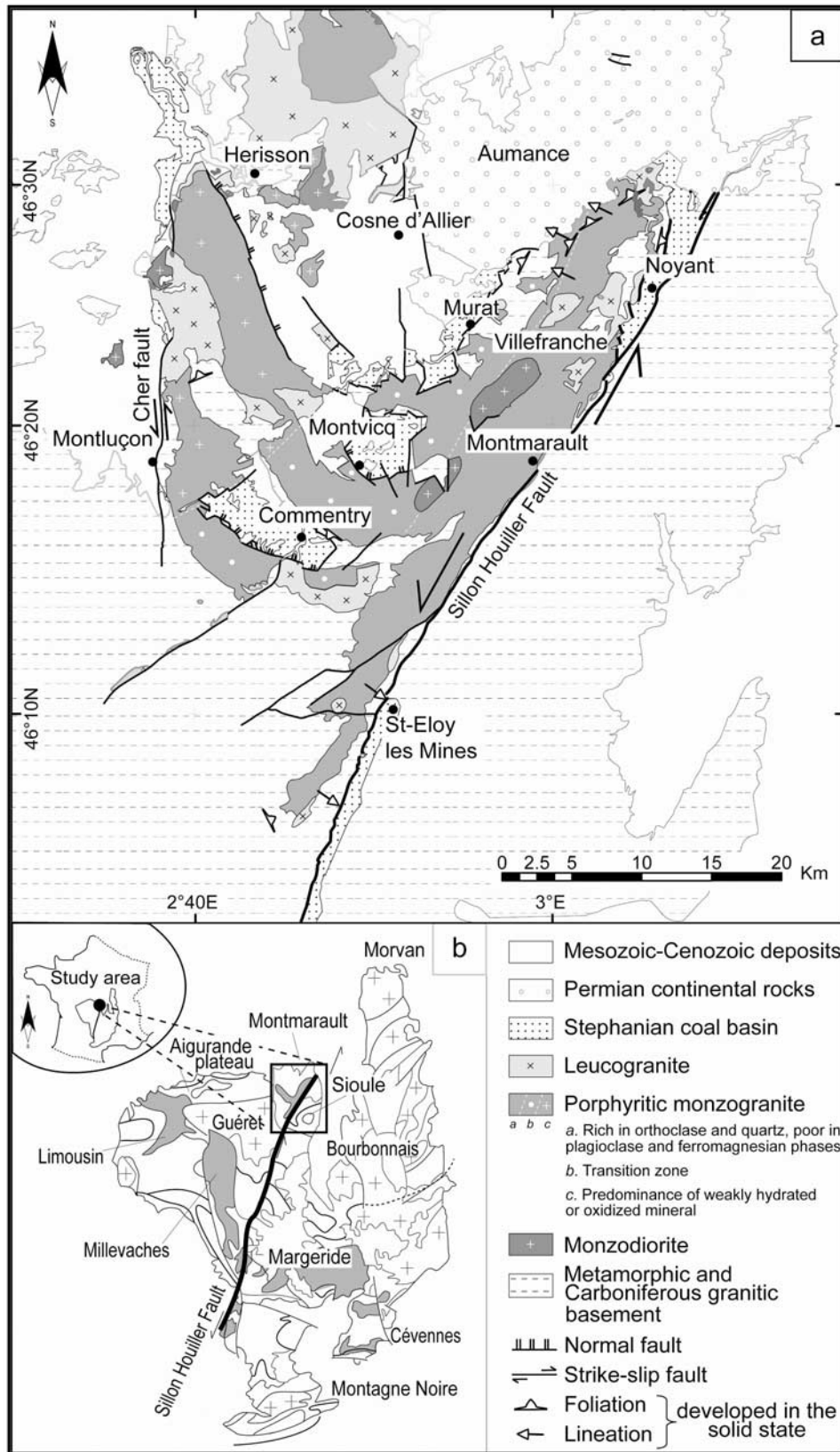


Figure 1. Structural map of (a) the Montmarault granitic pluton in (b) the French Massif Central.

placement. Moreover, the question of the structural and genetic relationships between fault and pluton is also addressed.

[3] Because of its particular tectonic position at the northern extremity of the FMC and along the SHF, the Montmarault granitic massif has been chosen as a target for this multidisciplinary study. Field structural analysis, petrological observation on thin section, monazite chemical U-Th-Pb dating, determination of anisotropy of magnetic susceptibility, gravity field measurement, interpretation of airborne survey, as well as three-dimensional (3-D) modeling have been carried out. The study is divided in two parts, this paper (hereinafter referred to as part 1) deals with geochronological dating, petrofabrics and AMS measurements followed by a discussion of the tectonic implications of our results with respect to the Late Variscan extension and to the activity of the SHF. The interpretations of new gravity measurements and previous aeromagnetic data as well as integrated 3-D geophysical modeling of the Montmarault granitic pluton described by *Joly et al.* [2007] (hereinafter referred to as part 2).

2. Geological Setting

2.1. Carboniferous Extensional Tectonics in the FMC

[4] The Variscan Belt of the FMC is a Paleozoic collisional orogen between the Gondwana and Laurussia plates [Matte, 1986; Ledru et al., 1989]. Crustal stacking has been followed by two distinct episodes of “crustal unthickening” accommodated by extensional tectonics, crustal melting, and erosion [e.g., Menard and Molnar, 1988; Faure, 1989, 1995; Malavieille et al., 1990; Faure and Pons, 1991]. The early stage is a synorogenic extension developed between 330 and 310 Ma, which is characterized by a NW-SE maximum stretching direction. The NW-SE extensional tectonics is diachronous throughout the FMC since in the north, extension started in Late Visean (circa 330 Ma), while in the south (i.e., Montagne Noire and Cévennes areas), at the same time, the compression was still active. In the southern FMC, the onset of this NW-SE extension occurred in Westphalian (circa 320–315 Ma). During this Middle Carboniferous NW-SE event, several synkinematic granitic plutons were emplaced [Faure, 1995; Talbot et al., 2004, and references therein]. In the northwestern Massif Central, the Middle Carboniferous magmatism is mainly represented by leucogranites whereas in the central and southern parts of the Massif Central (Cévennes and Margeride areas), the plutons are dominantly porphyritic monzogranites but both record the same NW-SE maximum stretching.

[5] The FMC experienced a second episode of extension characterized by N-S to NE-SW maximum stretching [Van den Driessche and Brun, 1989; Malavieille et al., 1990; Faure, 1995; Ledru et al., 2001]. Since this event occurred from Late Carboniferous to Early Permian, this second extensional tectonics is interpreted as a postorogenic gravitational collapse of the Variscan Belt [Menard and Molnar, 1988; Malavieille et al., 1990; Costa and Rey, 1995] due to the melting of the lower crust [Vanderhaege and Teyssier, 2001]. In the upper crust, the Late Carboniferous–Early Permian event is respon-

sible for the formation of intramountain coal basins, which are either half grabens or pull-aparts.

2.2. Geological Framework of the Montmarault Area

[6] The study area, located at the northern part of the FMC, immediately south of the unconformity of the Mesozoic cover of the Paris basin [Turland et al., 1989], is mostly occupied by the Montmarault granitic massif and its metamorphic host rocks which are locally overlain by Late Carboniferous to Permian coal basins (Figure 1a). In spite of extensive mapping and some limited petrological or structural works [Grolhier and Letourneur, 1968; Boissonas and Debeglia, 1976; Barbarin et al., 1985; Sossa-Simawango et al., 1987; Faure, 1995], the age, tectonic setting, architecture and emplacement mechanism of the Montmarault pluton are poorly constrained. Nevertheless, due to its northern location, the Montmarault pluton is potentially a suitable entity that might have recorded the extensional tectonics experienced by the FMC.

[7] In the study area, the Late Carboniferous (Stephanian) Commentry and Montvicq coal basins are half grabens. Their openings are controlled by NW-SE trending, NE dipping normal faults [Turland et al., 1989; Faure, 1995] developed along the southwestern boundary of each basin (Figure 1a). Moreover, the Late Carboniferous St-Eloy and Noyant basins (Figure 1a) opened along the left-lateral Sillon Houiller Fault (SHF) as pull-aparts during the N-S to NE-SW extensional tectonics. Therefore, during the Stephanian time, the SHF is a NNE-SSW trending strike-slip fault of more than 500 km in length along which several Stephanian coal basins formed coevally with fault displacement [Letourneur, 1953]. The cumulative strike-slip displacement is estimated at ~80 km [Grolhier and Letourneur, 1968; Bonijoly and Castaing, 1984; Blès et al., 1989]. Pre-Stephanian ductile activity of the SHF is not demonstrated yet. The SHF was interpreted as a transfer fault accommodating the late orogenic extension [Feybesse, 1981; Burg et al., 1990]; however, this assumption is not in accordance with two distinct and successive episodes of extensional tectonics [Faure, 1995].

2.3. Montmarault Pluton

[8] The Montmarault granitic pluton occupies an area of about 600 km². Its western margin corresponds to the Cher fault that bounds an Oligocene graben, and to the East, the Montmarault pluton is limited by the Sillon Houiller Fault (Figure 1a). The massif intrudes Late Devonian metamorphic rocks and the Guéret pluton (Figure 1b), which yields a Rb-Sr whole rock age of 356 ± 12 Ma [Berthier et al., 1979]. Recently, chemical U-Th-Pb dating on monazite from the Guéret pluton gives a 356 ± 5 Ma age that complies with previous Rb-Sr one (A. Cocherie, personal communication, 2006). To the north, the pluton is unconformably covered by Early Permian (Autunian) continental deposits of the Aumance basin, and is in fault contact with the Late Carboniferous (Stephanian) Murat coal basin. The present cartographic outline of the Montmarault massif does not correspond to the primary shape, since the pluton structure was partly disrupted by later tectonic events (tilting due to brittle faulting, Figure 1a) during the Late Carboniferous, Permian, and Mesozoic as well (compare part 2).

2.4. Granite Petrography

[9] The main part of the Montmarault massif consists of pink porphyritic monzogranite that locally encloses kilometer-scale monzodiorite septa and gneissic xenoliths similar to the country rocks. The monzogranite is cut by meter-scale leucogranite dikes and kilometer-scale leucogranitic stocks [Sossa-Simawango, 1980]. The leucogranites range from aplitic to pegmatic in texture and their mineralogical composition consists mainly of quartz, K-feldspar, plagioclase, muscovite and minor biotite. According to our structural observations, the leucogranites are younger than the porphyritic granite and were emplaced in a host granite already crystallized. The monzogranite also contains titanite and allanite rich mafic enclaves. The abundance of titanium and iron in the mafic enclaves argues for a lower crust origin for the magma source of the Montmarault monzogranite [Sossa-Simawango, 1980]. Petrological studies indicate a fast ascent of the magma throughout the middle crust and its emplacement close to the surface [Sossa-Simawango, 1980]. Moreover, first gravity investigations [Boissonas and Debeglia, 1976], the phase crystallization order, the presence of magnetite and the abundance of red orthoclase instead of microcline suggest a shallow depth (~ 2 km) for its emplacement [Turland et al., 1991].

[10] Two types of granitic facies, separated by a transition zone (Figure 1a), have been defined within the massif [Boissonas and Debeglia, 1976; Sossa-Simawango, 1980]. From a mineralogical viewpoint, the western part presents a predominance of weakly hydrated or oxidized minerals and, on the contrary, the eastern one is richer in orthoclase and quartz and poorer in plagioclase and ferromagnesian phases. Indeed, the western part is constituted by a porphyritic monzogranite with a magnetic susceptibility higher than in the eastern zone. As discussed below, these petrological insights are consistent with AMS and structural observations that support a deeper setting for the eastern part of the massif. Indeed, the presence of weakly hydrated or oxidized minerals suggests that the western part is closer to surface than the eastern part. Moreover, the gravity measurements (part 2) reinforce this assumption, since an intense negative gravity anomaly lies along the eastern domain whereas the western part of the pluton corresponds to a positive gravity anomaly. The Montmarault pluton is petrologically and geochemically similar to the Middle Carboniferous “red granites” of the Bourbonnais area (Figure 1b) that have been dated at $313 \pm 12/-9$ Ma by U-Pb method on zircon and at 318 ± 6 Ma and at 328 ± 4 Ma by Rb-Sr methods on whole rocks [Binon and Pin, 1989]. First chemical U-Th-Pb age on monazite for the Montmarault pluton is presented in section 3.

3. New U-Th-Pb Dating on the Montmarault Massif

[11] The age constraint is essential for the understanding of the relationships between Montmarault pluton emplacement and regional tectonic evolution. Whole rock Rb-Sr measurements on several facies of the Montmarault granitic pluton do not provide any conclusive isochron [Sossa-Simawango, 1980]. Over the past 15 years, owing to the technological progress on the electron microprobe measure-

ments, chemical geochronology realized on monazite has become possible [e.g., Suzuki and Adachi, 1991; Montel et al., 1996; Cocherie et al., 2005; Be Mezème et al., 2006a].

3.1. Analytic Procedure

[12] Because of its high U-Th contents and negligible common Pb content [Parrish, 1990], monazite constitutes one of the phases frequently used in geochronology. This use as radiochronometer is also enhanced by the restricted lead diffusion in monazite lattice [Montel et al., 1996, 2000] and by its high-temperature stability up to more than 900°C [Braun et al., 1998]. Monazite can record successive geological processes [e.g., Cocherie and Albarède, 2001; Be Mezème et al., 2006a]. In order to understand accurately the thermal and tectonic history experienced by a rock, geochronological data must be acquired in situ, that is to say, grains are directly analyzed with respect to their textural environment in thin section [Williams and Jercinovic, 2002]. Scanning electron microprobe (SEM) in back-scattered electron (BSE) mode is one of the best methods to distinguish constituent mineral species of the thin section. SEM allows us to recognize microinclusions, altered domains and all other components of non-monazite composition. Providing contrasted chemical composition of monazite, SEM can also help to define heterogeneous compositional domains, which can be related to inheritance phenomenon during successive episodes of crystallization. The detailed analytical procedure is described by Cocherie et al. [1998]. The theoretical procedure to reduce the data and to calculate the average age from individual spot analyses is given by Cocherie and Albarède [2001] and Cocherie et al. [2005]. None of the eight analyzed monazite grains exhibits optical or chemical zoning. This observation allows us to confidently assume that the Th, U and Th/U ratio variations correspond directly to crystallization time and thus grains should reveal homogeneous ages, as commonly the composition of the melt surrounding the monazite can significantly change during mineral growth [e.g., Be Mezème et al., 2005, 2006a]. The analyzed points correspond to the same event and the U-Th content variations will define an isochron in the geochronological representation (Th/Pb versus U/Pb diagram). Besides, as each point of the diagram corresponds to an age, it is possible to calculate an average age with good precision at the population centroid. Finally, mean squared weight deviation (MSWD) calculation must agree with the *Wendt and Carl* [1991] criteria to certify the statistical significance of the calculated average age.

[13] Porphyritic granite has been sampled at $46^\circ 19' 53.4''\text{N}$ and $2^\circ 45' 09.7''\text{E}$ for the geochronological study. This sample contains a common mineral composition of quartz, plagioclase, K-feldspar, biotite, zircon, apatite, monazite, xenotime, ilmenite, hematite and some iron oxides (magnetite, maghemite). Analyzed monazite grain sizes are between 50 and $100 \mu\text{m}$. The hand sample does not show any macroscopic mineral preferred orientation. Under the microscope in the dated sample, quartz grains reveal some weak undulose extinction and are almost free of subgrain boundaries. Biotites are not deformed. Ductile deformation is totally lacking in feldspars and compositional zoning of plagioclase is locally observed. These mineral microstruc-

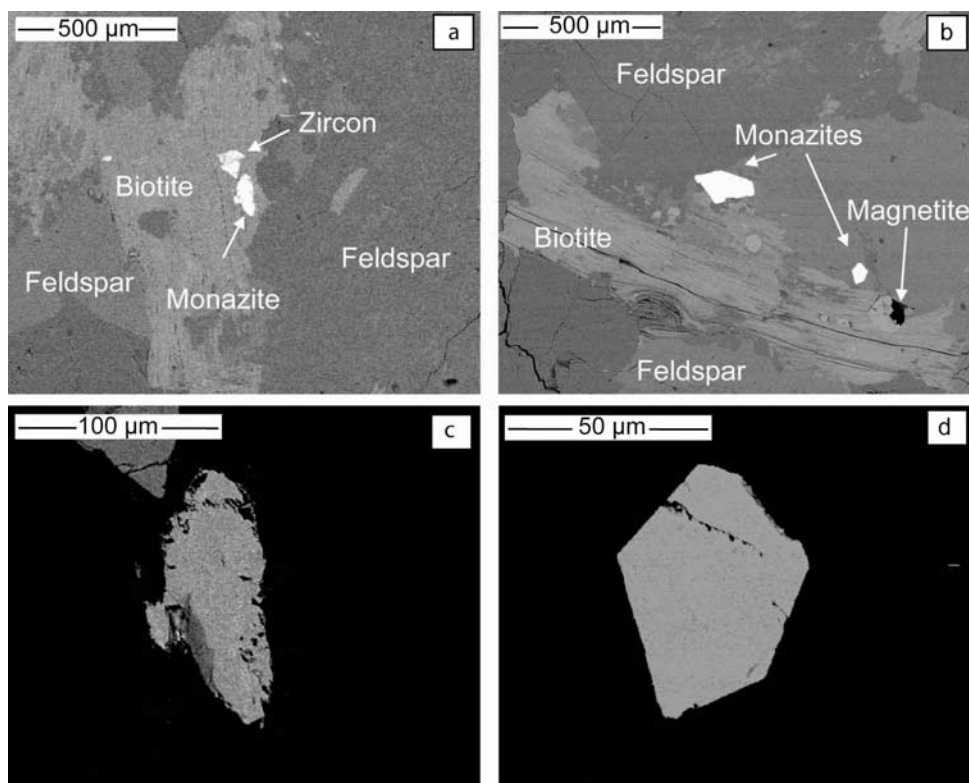


Figure 2. SEM images in BSE mode of representative monazite grains from the Montmarault granite. (a, b) Upper raw images that illustrate the textural relationships of monazite grains with the surrounding minerals. Monazite is included in biotite or along biotite grain boundaries. (c, d) Lack of U-Th zonation in monazite that complies with a single stage of crystallization.

tures are characteristic of a magmatic flow and indicate the lack of any solid-state deformation.

3.2. Dating Results

[14] As stated above, in the analyzed sample, the magmatic fabric is not overprinted by a postsolidus deformation. Therefore the obtained dating can be confidently considered as the crystallization age of the Montmarault granite coeval with its emplacement in its present outcropping site. Monazite is found as inclusions either in biotite (Figure 2a) or in feldspar (Figure 2b). Monazites grains are homogeneous without chemical zoning mainly related to U and Th contents (Figures 2c and 2d).

[15] Eight grains from one thin section of the porphyritic facies of the Montmarault massif were prepared and analyzed by a Cameca SX 50 EPMA cooperated by Bureau de Recherches Géologiques et Minières–Centre National de la Recherche Scientifique (BRGM-CNRS) and Orléans University. The analytic detection limits at 20 kV and 200 nA for U, Th, and Pb are of 105, 130, and 110 ppm, respectively, and they are considered as absolute errors. The 2σ errors given on individual ages depend on U, Th, and Pb contents and are calculated by propagating the uncertainties of these elements (with 95% confidence level) into the decay equation of *Montel et al.* [1996]. The analyses present a satisfactory accuracy with a MSWD of 0.68 inferior to 1 for 170 analyses [*Wendt and Carl, 1991*]. The intercept ages are well defined and consistent within errors, since the U-Pb

age (intercept with U-Pb axis) and the Th-Pb age (intercept with Th-Pb axis) are at $382 +73/-80$ Ma and $312 +11/-10$ Ma, respectively. Monazite grains yield a mean age of 321 ± 2 Ma (at 2σ confidence level; Figure 3). The calculated regression line, close to the theoretical isochron,

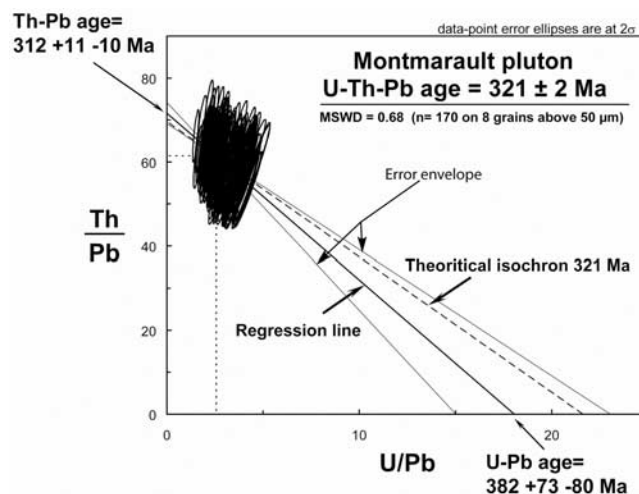


Figure 3. Th/Pb versus U/Pb isochron diagram for monazites from the Montmarault porphyritic granite.

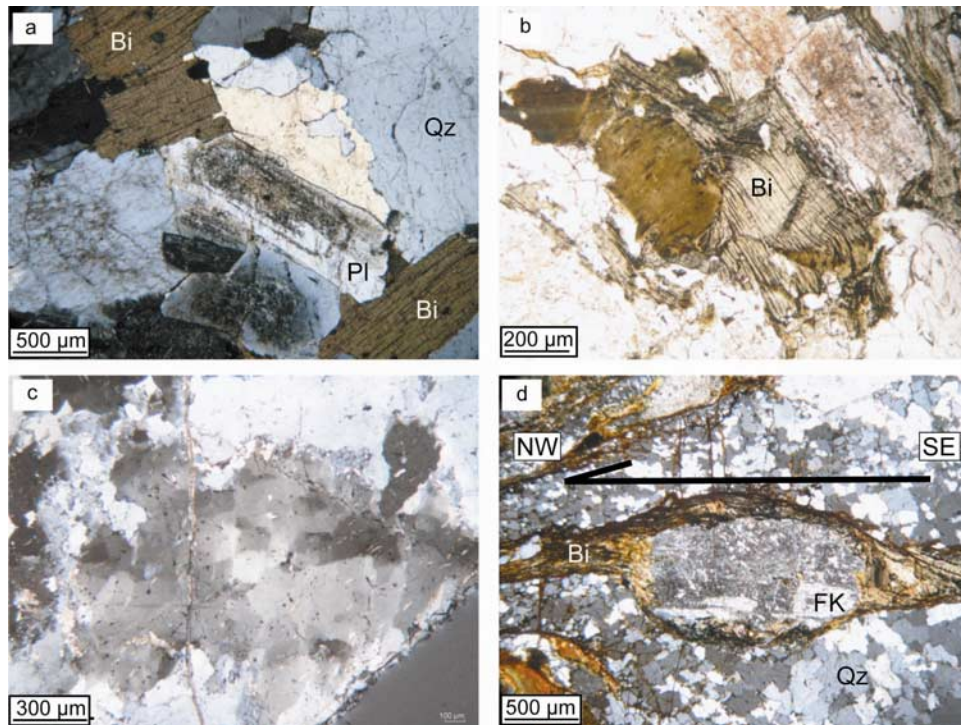


Figure 4. Characteristic microstructures for the microstructural domains as indicated on Figure 5. Thin sections are perpendicular to the magnetic foliation and parallel to the magnetic lineation defined by AMS study. (a) Magmatic domain where large and undeformed biotite grains (Bi) and quartz (Qz) coexist with zoned plagioclase (Pl); (b) and (c) weak solid state fabric; kinked biotite and undeformed feldspar (Figure 4b); quartz with chessboard pattern indicating both (a) and (c) dislocation slip activities during high-temperature deformation in porphyritic granite (Figure 4c); and (d) intense solid state fabric in granite mylonite showing ribbon of recrystallized quartz grain and sheared biotite. The folia anastomose around a deformed K-feldspar porphyroclast, the asymmetry indicates a top to the NW shearing.

indicates that the monazite grains experienced only one single crystallization event.

4. Rock Fabrics

4.1. Macroscopic Structures Within the Pluton

[16] In the Montmarault porphyritic pluton, K-feldspar fabrics present a variety of orientations [Barbarin *et al.*, 1985]. Except in the northwest boundary of the eastern branch, the preferred orientation of K-feldspar megacrysts shows a pronounced dip of the preferred orientation surface. The direction of foliation of K-feldspar is submeridian in the core of the pluton; it is deflected to an east-west orientation in the eastern part of the pluton. This change in trend is interpreted as the evidence for a late event of plastic deformation [Barbarin *et al.*, 1985]. The northwest boundary of the eastern branch of the pluton is mylonitized and associated to a flat lying foliation containing a N150°E trending stretching lineation. In sections perpendicular to the foliation and parallel to the lineation, kinematics indicators such as sigma-type porphyroclast systems, sigmoidal biotite or S-C fabrics indicate a top-to-the NW shearing (Figure 1a). The mylonitization occurred during or after the granite crystallization, i.e., in Namurian (320 Ma), and before the deposition of the Early Permian sandstone that unconformably covers the mylonite [Faure, 1995]. Thus,

except in the northeastern part of the massif, the Montmarault pluton exhibits undeformed minerals. This is the reason why the techniques of petrographic fabrics and the anisotropy of magnetic susceptibility (AMS) were applied in this study.

4.2. Mineral Fabrics

[17] Detail examinations of rock fabrics and mineral microstructures of magmatic rocks have been proposed for a long time to understand the kinematic and dynamic patterns of plutons related to their crystallization and emplacement; and to reconstruct the tectonic setting experienced by the crust at the time of pluton emplacement [e.g., Hibbard, 1987; Paterson *et al.*, 1989; Vernon, 2000, and references therein]. It is well acknowledged that microstructures record the evolution of the rheologic state of the magma during the experienced cooling of the magma as well as plastic deformation in solid state. Indeed, the rheologic state is changing when magma crystallization evolves from a linear viscous behavior corresponding to low content of crystals to a Bingham behavior matching to higher crystal content. Magmatic flow may be defined as the deformation by displacement of melt with consequent rigid body rotation of crystals [Paterson *et al.*, 1989; Vernon, 2000]. Oppositely, solid state deformation is characterized by intracrystalline plastic deformation, dynamic

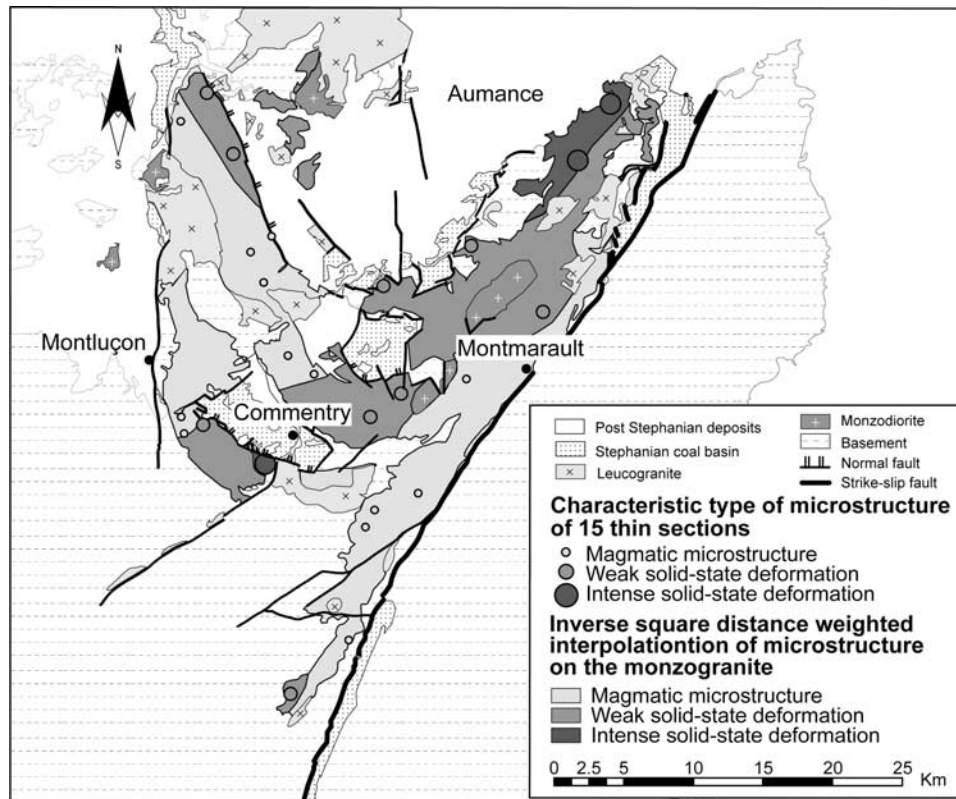


Figure 5. Deformation domains within the Montmarault pluton.

recrystallization and at lower temperature by appearance of cataclastic flow of high-strength minerals such as feldspars or amphiboles.

[18] On the basis of detail analyses of 15 thin sections by optical microscope, three principal microstructural types are distinguished in the Montmarault pluton.

[19] 1. The dominant type is a magmatic fabric characterized by an equigranular arrangement of large quartz grains with no intragranular microstructure (Figure 4a). Undulatory quartz extinction is not observed but euhedral plagioclase crystals with synneisus association between grains exist. Large brown biotites with opaque inclusions (magnetite, ilmenite) are not deformed. These microstructures are interpreted as primary because the feldspar grains preserved their initial compositional zoning and lack evidence of either ductile or brittle solid-state deformation. Rare myrmekites within orthoclase are interpreted as the result of crystallization of water saturated magma [Hibbard, 1987]. In this microstructural type, some small sized magnetite grains are observed with their primary shapes.

[20] 2. Weak solid-state deformation is the transitional rheological state between magmatic and solid states. This fabric is characterized by the limited kinking of few grains of biotite (Figure 4b). Myrmekites in feldspar are rare. Quartz grains exhibit a conspicuous undulatory extinction and rare dynamic recrystallization. Indeed, numerous small-sized quartz grains develop at the expense of a large porphyroblast that shows a chessboard texture (Figure 4c) formed by the coeval activity of both (a) and (c) dislocation slip. These microstructures formed under high-temperature

conditions during granitic magma crystallization and are considered as evidence of a weak solid-state deformation.

[21] 3. Intense solid-state structure is rarely observed in the Montmarault pluton, but it is conspicuous in the mylonites that crop out in the northwest part of the eastern branch of the massif. It is characterized by a severe intracrystalline plastic deformation. Quartz grain size reduction due to dynamic recrystallization is well developed. The neograins are arranged in a ribbon pattern and often exhibit an oblique shape fabric. Highly sheared biotites anastomose around weakly deformed but recrystallized K-feldspar porphyroclasts. It is worth noting that sigmoidal biotite, quartz oblique shape fabric and sigma-type porphyroblast systems comply with the top-to-the-NW shearing observed at the outcrop scale (Figure 4d) associated to a flat lying foliation containing a N150°E trending stretching lineation.

[22] At the pluton scale, the distribution of these different types of microstructures shows a well defined spatial organization (Figure 5). The Montmarault pluton is dominantly characterized by magmatic (50%) and weak solid-state deformation (40%) primary microstructures. Magmatic microstructures predominate in the zone located along the SHF and in the western part of the pluton while weak solid-state deformation spreads out in a NE-SW direction from the core of the pluton to its extreme northwestern part. In the northwest part of the eastern branch of the massif, the granitic rocks present an intense planar and linear fabric. This is the only part of the massif where the intense solid-state microstructures are significantly developed. This area corresponds to the mylonitic margin of the pluton with a

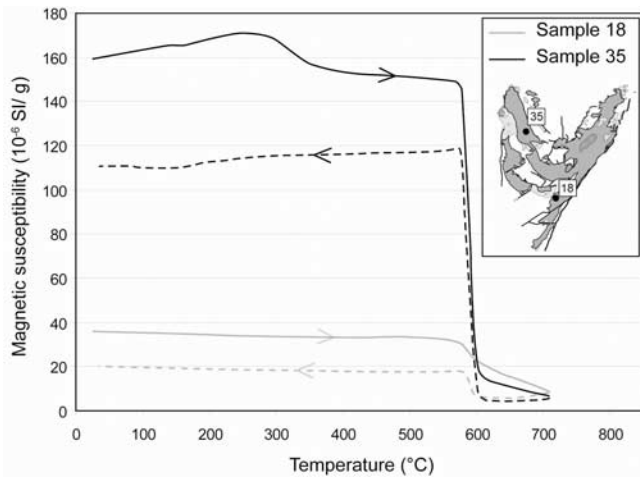


Figure 6. Thermomagnetic curves in free air for two representative samples. The rapid decrease of magnetic susceptibility at about 580° indicates the presence of magnetite. Solid (dotted) lines stand for heating (cooling) curves.

top-to-the NW shearing (Figure 4d). Locally, important undulose extinction of some quartz grains is observed in the footwall of the fault that underlies the Commeny coal basin along its SW margin (Figure 1a). This limited ductile

deformation, superimposed on a magmatic fabric, is likely related to the activity of the listric normal fault controlling the opening of the Commeny half graben [Faure, 1995].

4.3. Magnetic Fabrics

[23] Providing a rapid insight of the bulk internal structure of a pluton and facilitating the definition of fabric elements, the Anisotropy of Magnetic Susceptibility (AMS) is considered as the most efficient method to study the fabrics in weakly deformed rocks [e.g., Hrouda, 1982]. AMS is therefore widely used for the analysis of both solid-state fabrics and the more subtle magmatic fabrics in granitoids [e.g., Bouchez, 1997].

4.4. Magnetic Mineralogy

[24] Before AMS determinations, several methods were employed to identify the magnetic mineral composition: thermomagnetic experiments, X-ray diffraction analyses, hysteresis loops, and isothermal remanent magnetization.

[25] Because of their locations, five representative samples have been selected for thermomagnetic experiments carried out by an AGICO KLY3 Kappabridge–CS3 furnace apparatus in the Laboratory of Rock Magnetism of Orléans University (France). The presence of magnetite seems evident with significant drops at about 580°C (Figure 6). However, the concentration of this mineral is remarkably lower in the eastern part with respect to the western one as

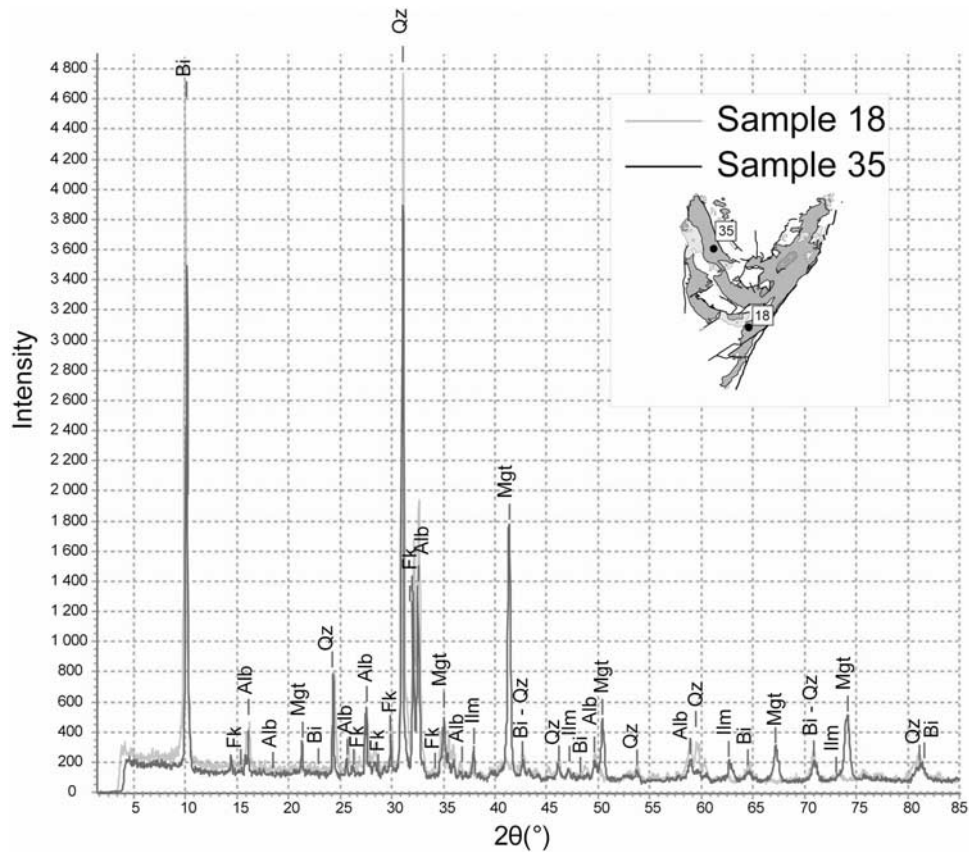


Figure 7. Representative X-ray diffraction spectra of powder of two samples from the porphyritic Montmarault granite with the interpretation of mineral composition. Qz, quartz; Fk, K-feldspar; Bi, biotite; Alb, Albite; Mgt, magnetite; Ilm, ilmenite.

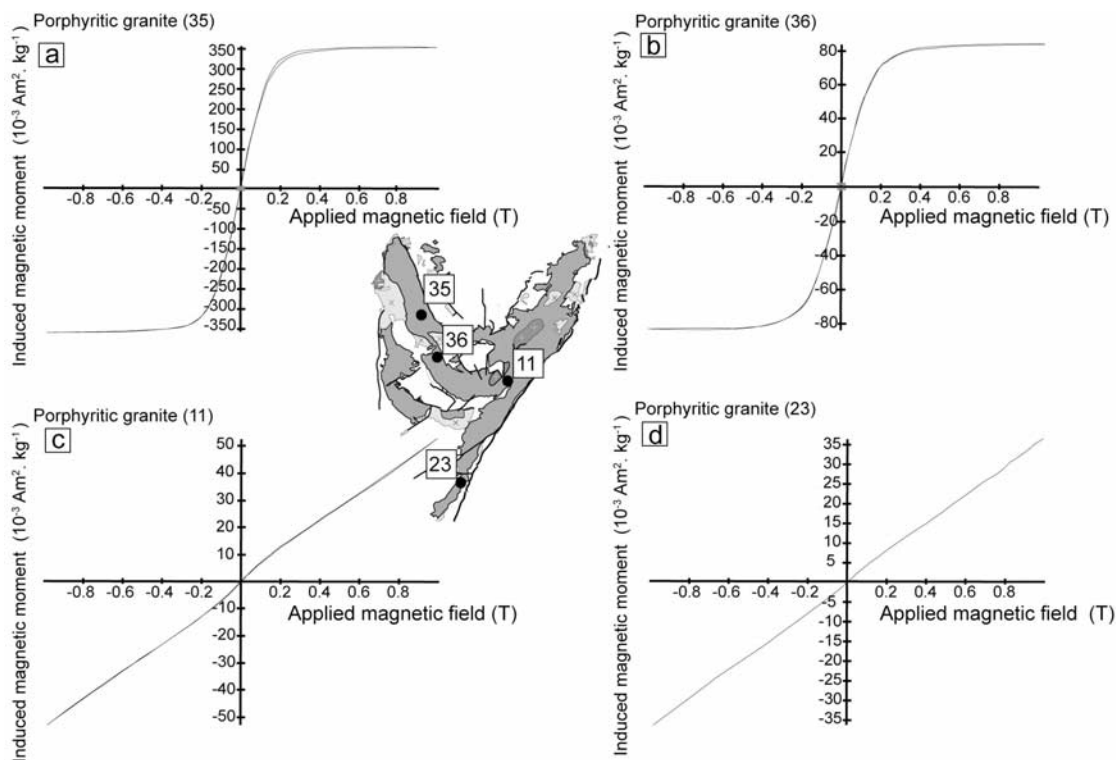


Figure 8. Hysteresis curves in field up to 1 T of 4 samples of porphyritic granite illustrating the presences of (a, b) ferrimagnetic sensu lato and (c, d) paramagnetic minerals.

the thermomagnetic curves are normalized to mass of samples (Figure 6).

[26] Ten X-ray diffraction analyses with an INEL diffractometer with a cobalt tube and a XRG 3000 generator and microscopic observations carried out in Institut des Sciences de la Terre d'Orléans show a relatively common composition for the entire pluton on the majority of minerals, such as quartz, biotite, K-feldspar, albite (Figure 7). However, the abundance of magnetite in samples from the western part of the pluton has been demonstrated (e.g., sample 35 in Figure 7). This result is confirmed by optical observation on thin sections (Figure 2b).

[27] Six hysteresis loops on several representative specimens were determined using a translation inductometer within an electromagnet providing a field of up to 1 T at the Paleomagnetic laboratory of Institut de Physique du Globe de Paris at Saint Maur. Two types of magnetic behavior are identified. Hysteresis curves of the first type for the samples from the western part of the pluton present ferromagnetic sensu lato minerals with magnetic saturation at about 300 mT (Figures 8a and 8b). This shows the presence of magnetite as a significant magnetic mineral. The form of the curve, without apparent inflections, suggests that the grain size is homogeneous [Tauxe *et al.*, 1996]. The ratios of H_{rs}/H_r and M_{rs}/M_r indicate that magnetite is principally multidomain [Day *et al.*, 1977]. It is worth noting by optical observation that magnetite is often found in inclusion in biotite and is sometimes substituted by ilmenite that begins to be altered into hematite and iron oxide mixture. Its 5–30 μm size is sufficient to strongly increase the magnetic susceptibilities, even if magnetite is

rare. For the samples from the eastern part, near the SHF, Figures 8c and 8d show the typical behavior of paramagnetic minerals with very slight flex up to 0.15 T and almost perfect linear variation of induced magnetic moment by increasing and decreasing magnetic fields up to 1 T, indicating the paramagnetic minerals as the principal magnetic carriers. Thus the magnetic mineral analyses indicate that magnetite grains control the magnetic fabrics of the western part of the pluton, despite the presence of several other magnetic mineral phases, including ilmenite, hematite as well as iron silicates. However, the paramagnetic minerals, such as biotite, are the main AMS carriers for the eastern part near the SHF.

4.5. AMS Measurements

[28] For the AMS study of the Montmarault pluton, 295 cores were collected from 54 sites (49 sites of monzogranite and 5 sites of leucogranite) covering the whole pluton using a portable gasoline drill. When it was possible, the cores were oriented, both by magnetic and sun compasses. The mean difference between magnetic and sun azimuths was less than 0.5° . The cores were cut into the standard specimens of 22 mm in length and 25 mm in diameter. The AMS measurements (Table 1) were carried out by an AGICO Kappabridge KLY 3S apparatus in the Laboratory of Rock Magnetism of Orléans University. Figure 9 shows the histogram distribution of bulk magnetic susceptibility values ($K_m = (K_1 + K_2 + K_3)/3$) characterized by a single mode at about 150 μSI with a long queue until about 7500 μSI . This typical 150 μSI value is widely observed among the numerous granitic plutons where

Table 1. Data of Anisotropy of Magnetic Susceptibility Obtained From This Study^a

Site	Type	Latitude	Longitude	n	BMS	K ₁				K ₃				P _j ^b	T
						Dec	Inc	a95min	a95max	Dec	Inc	a95min	a95max		
MM1	porphyritic granite	46°21'2.5"	2°59'49.8"	4	675	4.9	28.7	15.1	18.0	205.2	61.0	5.2	18.8	1.142	0.252
MM2	porphyritic granite	46°21'2.0"	2°59'49.8"	5	245	23.2	40.4	7.1	20.2	182.0	45.3	6.5	12.4	1.058	0.014
MM3	porphyritic granite	46°21'1.5"	2°59'49.8"	6	575	26.5	47.5	9.5	12.2	203.0	45.0	8.0	27.8	1.117	-0.108
MM4	porphyritic granite	46°24'0.6"	2°54'27.6"	5	4098	317.1	3.0	4.3	18.3	50.6	59.1	2.3	6.8	1.250	0.440
MM5	porphyritic granite	46°24'0.6"	2°54'37.0"	5	901	281.0	34.1	20.5	32.1	45.1	39.6	17.1	23.7	1.093	-0.011
MM6	porphyritic granite	46°24'1.0"	2°54'37.0"	6	5113	276.6	41.0	7.4	26.0	40.8	35.2	7.0	10.4	1.311	0.511
MM7	porphyritic granite	46°21'31.4"	2°55'02.2"	3	4814	235.5	12.8	12.2	20.0	2.8	73.3	11.8	23.1	1.178	0.514
MM8	porphyritic granite	46°22'3.4"	2°50'44.1"	6	120	133.0	10.6	14.1	18.0	228.6	16.3	11.1	23.0	1.017	-0.055
MM9	porphyritic granite	46°22'34.4"	2°50'31.8"	7	96	126.7	11.4	13.5	27.0	26.9	49.2	7.6	20.6	1.019	0.337
MM10	porphyritic granite	46°10'33.7"	2°53'59.3"	5	378	82.4	68.0	7.9	17.4	328.1	8.5	3.1	10.9	1.157	0.481
MM11	porphyritic granite	46°18'56.3"	2°55'7.3"	5	169	244.3	66.3	10.5	15.8	141.5	6.1	8.8	13.7	1.035	0.743
MM12	porphyritic granite	46°16'24.1"	2°53'31.9"	5	130	160.8	39.5	2.8	11.5	328.9	51.4	1.5	13.9	1.026	-0.579
MM13	porphyritic granite	46°13'28.7"	2°52'55.8"	6	175	63.6	79.6	7.8	16.1	316.2	4.4	5.9	16.7	1.037	0.175
MM14	porphyritic granite	46°14'31.7"	2°52'23.3"	4	304	41.1	30.2	8.7	25.8	256.9	56.0	3.3	14.6	1.048	0.223
MM15	porphyritic granite	46°13'53.3"	2°49'57.2"	6	1066	64.3	3.0	11.0	32.8	335.3	21.6	6.9	12.5	1.127	0.670
MM16	porphyritic granite	46°14'18.8"	2°49'9.4"	6	379	269.8	10.6	9.3	27.4	3.6	28.1	5.6	13.4	1.068	0.389
MM17	porphyritic granite	46°13'34.8"	2°49'22.7"	6	1975	119.8	43.0	14.1	43.3	357.9	14.8	6.3	20.2	1.076	0.757
MM18	porphyritic granite	46°13'13.7"	2°49'25.9"	6	114	254.0	47.3	10.0	35.9	358.0	10.1	10.4	25.7	1.017	0.378
MM19	porphyritic granite	46°11'45.5"	2°48'45.5"	6	1248	221.2	61.8	7.0	33.0	313.7	0.4	7.6	11.6	1.038	0.710
MM20	leucogranite	46°10'10.7"	2°48'5.8"	6	122	93.3	50.7	8.2	36.7	334.1	14.8	11.2	14.9	1.014	0.694
MM21	porphyritic granite	46°8'51.1"	2°48'27.9"	4	57	143.7	69.3	5.6	17.3	283.4	13.4	0.3	38.4	1.063	-0.042
MM22	porphyritic granite	46°8'21.7"	2°48'15.6"	6	58	187.7	49.6	7.0	32.0	326.7	27.7	10.0	27.7	1.033	0.382
MM23	porphyritic granite	46°8'43.5"	2°47'42.1"	5	126	98.2	40.4	4.0	41.2	333.3	34.6	3.0	6.1	1.126	-0.262
MM24	porphyritic granite	46°8'30.0"	2°47'4.0"	5	84	96.2	29.1	10.4	33.7	336.0	37.9	5.1	11.5	1.019	0.766
MM25	porphyritic granite	46°7'28.4"	2°45'57.1"	3	84	129.3	49.6	7.9	19.7	327.3	37.6	5.5	9.5	1.031	0.874
MM26	porphyritic granite	46°6'46.9"	2°45'12.6"	5	111	160.1	26.7	3.4	9.2	23.5	54.1	2.3	13.1	1.029	0.317
MM27	porphyritic granite	46°12'49.9"	2°48'40.4"	6	1155	277.5	33.7	11.3	34.0	189.8	1.5	5.6	12.1	1.165	0.614
MM28	porphyritic granite	46°15'42.1"	2°43'51.6"	6	4632	195.8	45.6	4.1	6.5	30.5	44.0	5.9	14.3	1.178	-0.032
MM29	porphyritic granite	46°17'13.5"	2°40'24.7"	5	1425	40.8	58.4	2.8	5.3	247.0	29.0	4.1	2.3	1.161	0.219
MM30	joint+porphyritic granite	46°16'53.2"	2°39'20.7"	6	1586	2.4	46.3	2.6	26.3	228.5	33.7	2.0	4.9	1.129	0.790
MM31	porphyritic granite	46°17'32.2"	2°39'11.0"	5	134	97.7	61.0	7.4	45.7	237.5	20.5	4.1	9.8	1.028	0.841
MM32	porphyritic granite	46°18'30.6"	2°38'38.1"	6	179	110.0	19.3	8.3	42.5	224.0	35.2	6.3	15.5	1.045	0.610
MM33	leucogranite	46°22'53.3"	2°38'7.3"	5	30	272.9	5.3	7.7	10.3	162.9	59.0	5.0	41.2	1.077	-0.676
MM34	porphyritic granite	46°24'31.0"	2°44'17.1"	6	5044	266.1	47.9	6.6	11.0	52.2	38.3	4.3	9.6	1.102	0.117
MM35	noporphyritic granite + enclave	46°23'52.1"	2°43'10.3"	7	7195	70.4	-52.6	4.4	18.9	63.4	34.9	5.6	12.0	1.108	0.291
MM36	porphyritic granite	46°19'53.4"	2°45'9.7"	8	1537	286.4	17.4	6.7	28.4	69.7	71.2	9.4	13.6	1.117	0.557
MM37	porphyritic granite	46°19'38.0"	2°46'37.3"	7	284	211.7	33.3	2.4	14.7	40.2	57.1	1.5	3.8	1.069	0.598
MM38	porphyritic granite	46°17'29.9"	2°49'45.1"	6	2886	126.7	70.9	5.5	14.0	9.3	9.7	3.6	5.9	1.093	0.475
MM39	porphyritic granite	46°18'6.8"	2°50'24.1"	8	172	101.1	77.1	8.5	18.4	350.1	5.2	7.3	26.0	1.021	-0.138
MM40	porphyritic granite	46°18'24.4"	2°51'34.2"	7	270	247.8	76.4	5.4	16.1	356.7	3.8	3.8	6.9	1.096	0.427
MM41	porphyritic granite	45°19'36.3"	2°53'53.7"	6	3804	137.5	52.7	6.0	19.2	308.9	39.0	6.5	19.9	1.167	0.234
MM42	porphyritic granite	46°17'32.5"	2°51'15.9"	6	1673	345.7	66.2	2.2	16.5	204.0	20.2	9.0	20.5	1.098	-0.139
MM43	porphyritic granite	46°18'4.3"	2°50'49.0"	6	953	129.0	75.1	2.1	13.1	0.9	8.9	2.8	17.8	1.117	0.406
MM44	porphyritic granite	46°20'46.1"	2°45'17.9"	4	2200	109.9	21.6	9.4	35.2	359.2	38.1	3.7	15.3	1.138	0.287
MM45	leucogranite	46°21'44.2"	2°45'29.0"	5	31	342.9	62.9	2.7	6.7	203.3	30.1	6.5	44.5	1.126	0.625
MM46	porphyritic granite	46°22'58.1"	2°43'38.7"	6	7486	246.2	47.1	4.7	12.2	54.0	43.3	4.6	11.5	1.095	-0.010
MM47	porphyritic granite	46°24'31.6"	2°43'47.4"	6	4015	275.1	52.3	2.1	5.8	42.1	24.5	1.3	6.9	1.134	0.297
MM48	leucogranite	46°23'54.4"	2°40'06.6"	5	48	256.4	44.7	7.3	12.1	134.5	29.0	10.9	17.6	1.018	0.005
MM49	porphyritic granite	46°27'54.5"	2°42'11.6"	6	1320	272.0	45.8	2.9	9.6	45.9	34.0	1.8	4.5	1.256	0.229
MM50	porphyritic granite	46°29'11.0"	2°39'15.0"	6	4771	187.2	55.1	3.5	7.1	73.0	15.7	3.1	5.5	1.176	0.302
MM51	porphyritic granite	46°30'16.3"	2°40'37.5"	4	3731	193.8	41.7	1.1	23.5	81.5	23.8	1.2	4.7	1.170	0.576
MM52	porphyritic granite	46°20'50.5"	2°44'49.3"	5	5579	54.1	4.8	2.8	9.5	179.1	81.8	1.6	3.3	1.221	0.100
MM53	leucogranite	46°27'50.8"	2°44'53.8"	4	55	252.7	32.1	8.1	10.6	82.2	50.9	1.7	12.9	1.058	0.455
MM54	porphyritic granite	46°27'15.5"	3°02'43.8"	4	157	287.8	29.6	4.1	23.0	90.2	58.1	0.9	18.6	1.042	0.229

^aHere n is number of measured specimens; BMS is bulk magnetic susceptibility in 10⁻⁶ SI; Dec, Inc, a95min, a95max are declination, inclination, maximal, and minimal 95% confidence intervals from *Bingham* [1964] bimodal statistics, respectively, in degree; P_j is corrected anisotropy degree; and T is ellipsoid shape parameter [Jelinek, 1981; Hrouda, 1982].

^bP_j = exp {2 [(ln K₁ - ln K₃)² + (ln K₂ - ln K_{mean})² + (ln K₁ - ln K_{mean})²]}^{1/2} with K_{mean} = 1/3 (K₁ + K₂ + K₃) and T = [2 ln (K₂/K₃)/(ln (K₁/K₂))] - 1.

paramagnetic minerals are the main contributors of magnetic susceptibility [e.g., *Ellwood and Wenner*, 1981; *Zapletal*, 1990]. However, these wide-ranged high values may show heterogeneous behavior of magnetite probably due to crystallization process. The sites that possess low magnetic susceptibility values (<600 μSI) are essentially located in the eastern part of the pluton along the SHF, whereas the

sites of high values (>600 μSI) are mainly located in the western area. Leucogranites yield weaker values of magnetic susceptibility (<150 μSI) which is also in agreement with the abundance of paramagnetic minerals (Table 1). In consideration of relative content between the white or black micas, the magnetic mineralogy of leucogranite is due to the

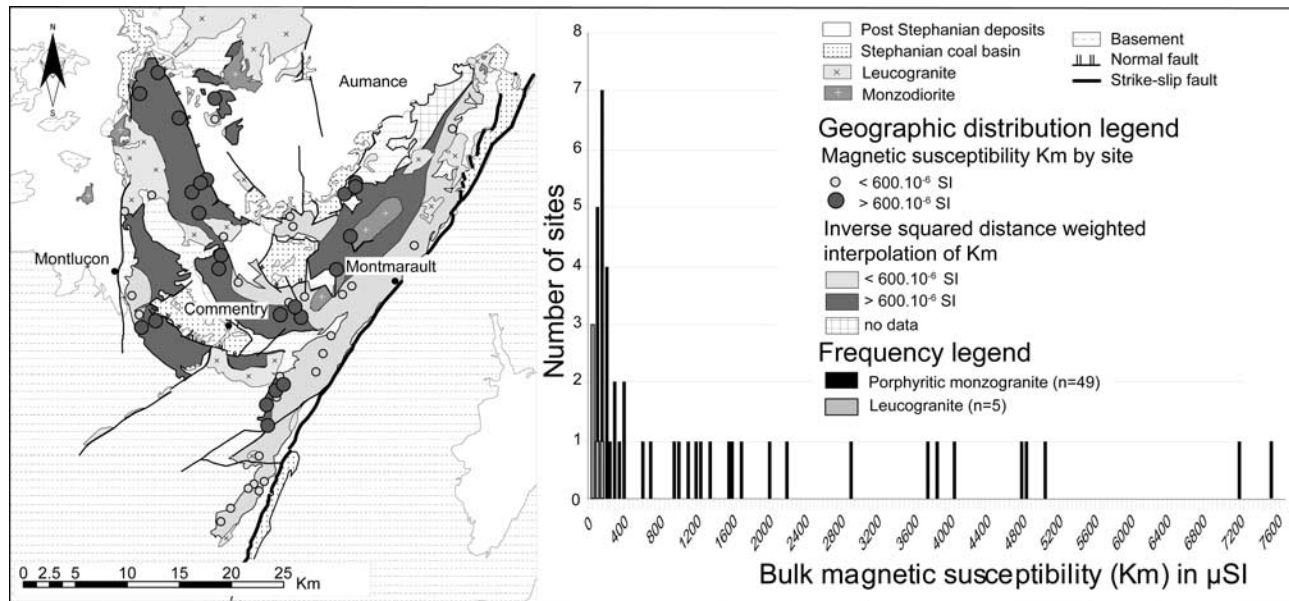


Figure 9. Geographic distribution and frequency histogram of bulk magnetic susceptibility, km.

contribution of both biotite and iron-bearing muscovite or only the iron-bearing muscovite.

[29] After the measurements of induced magnetization in different directions in a weak magnetic field, the three principal axes of the shape ellipsoid are defined by a tensor calculation for each specimen ($K_1 > K_2 > K_3$; see Figure 10). Being long and short axes of the ellipse, K_1 and K_3 are considered as the magnetic lineation and the pole of magnetic foliation, respectively. For each site, a mean direction for each of these three principal axes is calculated with a corresponding confidence interval at the 95% level by Bingham's [1964] statistic method (Table 1 and Figure 10). Concerning the AMS directional distribution, more than 80% of sampled sites reveal at least one well-defined axis with a confidence level less than 20° (Figure 10). If confidence level of a magnetic axis, K_1 and/or K_3 , is larger than 20° within a site, this magnetic axis is considered as poorly defined, and thus the site-average orientation is not reliable (Table 1).

[30] Four groups of sites can be distinguished. Namely, group I (45%) is characterized by three well clustered axes (e.g., sites 10 and 50 in Figure 10), group II (13%) corresponds to the sites where K_1 is better defined than K_2 and K_3 (e.g., site 33 in Figure 10), group III (33%) shows the opposite case to group II, K_3 is better clustered than other two axes (e.g., site 23 in Figure 10), group IV (9%) presents three scattered axes (e.g., site 18 in Figure 10). The secondary AMS related to solid-state deformation will not be taken into account because they are associated with syngranite to postgranite deformation (Figure 5).

[31] In order to better understand the AMS fabric pattern observed in this pluton, the degree of anisotropy (P_j) and shape parameter (T ; see Figures 11 and 12) have been calculated according to Jelínek [1981]. The shape parameter T (Figure 11b) represents the degree to which the fabric ellipsoid is prolate ($0 > T > \text{or} = -1$) or oblate ($0 < T < \text{or} = 1$). 92% of the sites present an anisotropy degree P_j lower than

1.2, and 80% of the sites show a T parameter between 0 and 1 (Table 1 and Figure 12). The T value shows a dominance of the AMS oblate ellipsoids (Figure 11b). A spatial correlation between the magnetic susceptibility (Figure 9) and the degree of anisotropy (Figure 11a) exists, particularly in the western part of the pluton. Variations of P_j are likely partly related to the magnetic mineralogy, i.e., either due to the magnetite or biotite [Borradaile and Henry, 1997].

[32] Figures 13a and 13b present the magnetic foliation and lineation distribution patterns, respectively. Only statistically well defined data are presented on the maps with the confidence level lower than 20° (Figure 13 and Table 1). In the eastern part of the pluton, that stretches parallel to SHF, the magnetic fabrics are mainly characterized by a dominant NE-SW trending foliation with steeply plunging dips toward the SE (40° to 90° ; Figure 13a) and by a well defined NW-SE trending magnetic lineation plunging mainly to the southeast at about 72° perpendicularly to the SHF (see maximum density in Figure 13b). In the central part of the Montmarault pluton, the NE-SW trending foliation is bent in an E-W direction. This magnetic fabric pattern correlates well with the previous measurements (Figure 13) carried out only on the northeastern part of the Montmarault pluton by Sossa-Simawango *et al.* [1987]. In the other parts of the pluton, the NNW-SSE magnetic foliations are roughly perpendicular to the SHF (Figure 13a). In the northwest area of the Montmarault massif, the magnetic foliation is gently dipping about 42° to the southwest and generally, the NW-SE magnetic lineation plunges to the west (48°). To the south of Commentry, in the southwestern part of the massif, the well defined magnetic foliation with also a NW-SE strike dips 60° to the northeast. However, the magnetic lineations are too scattered to define a statistically reliable orientation (Figure 13b).

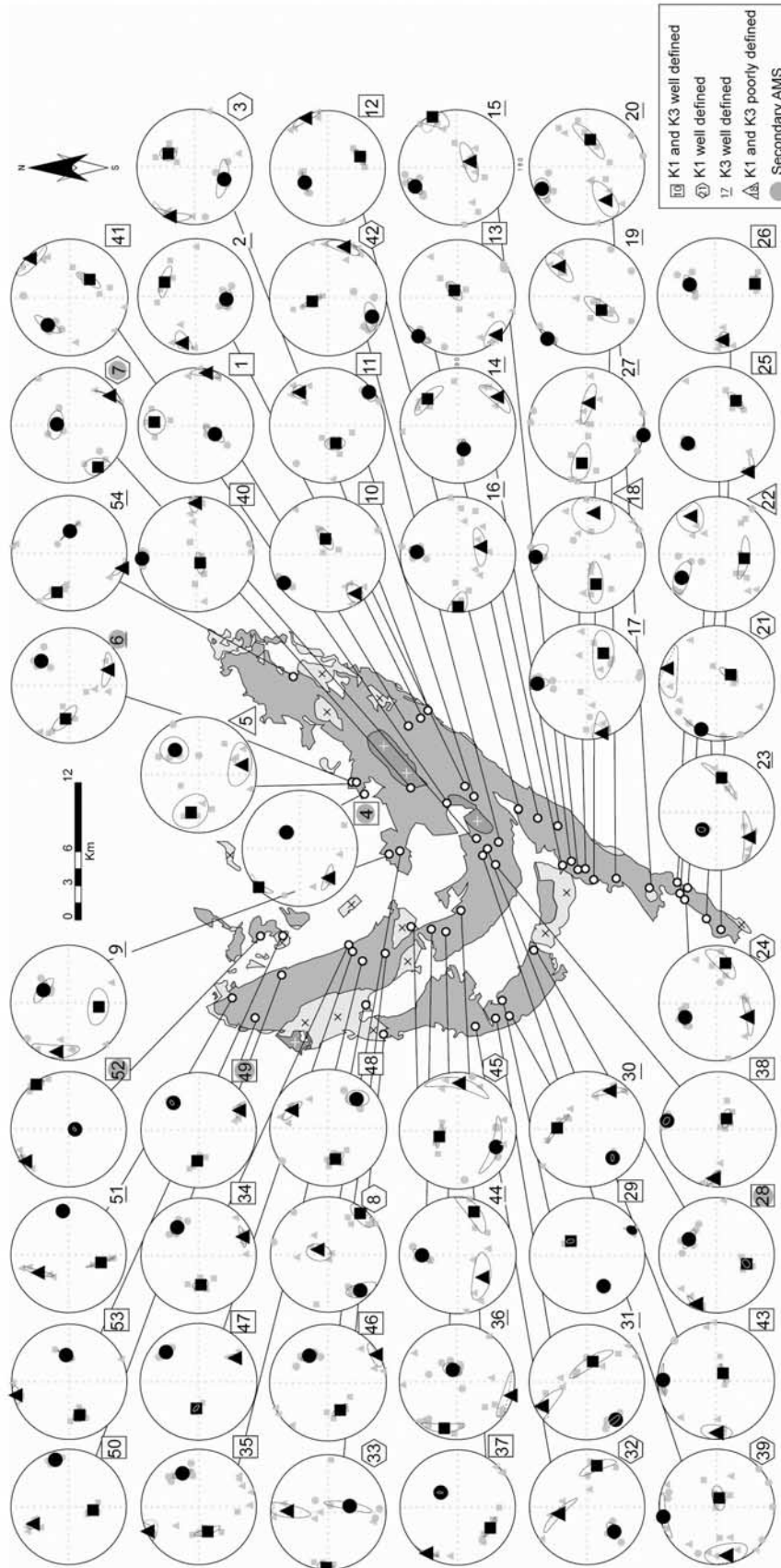


Figure 10. Equal-area, lower hemisphere projection of the directions of the magnetic susceptibility axes from 54 sites with their geographical corresponding location within the Montmarault pluton. The three main axes of ellipsoid (K₁, K₂, and K₃) are represented by square, triangle, and circle, respectively, with 95% confidence zone. Small grey symbols are for the specimen data; the large black symbols are for the average site data.

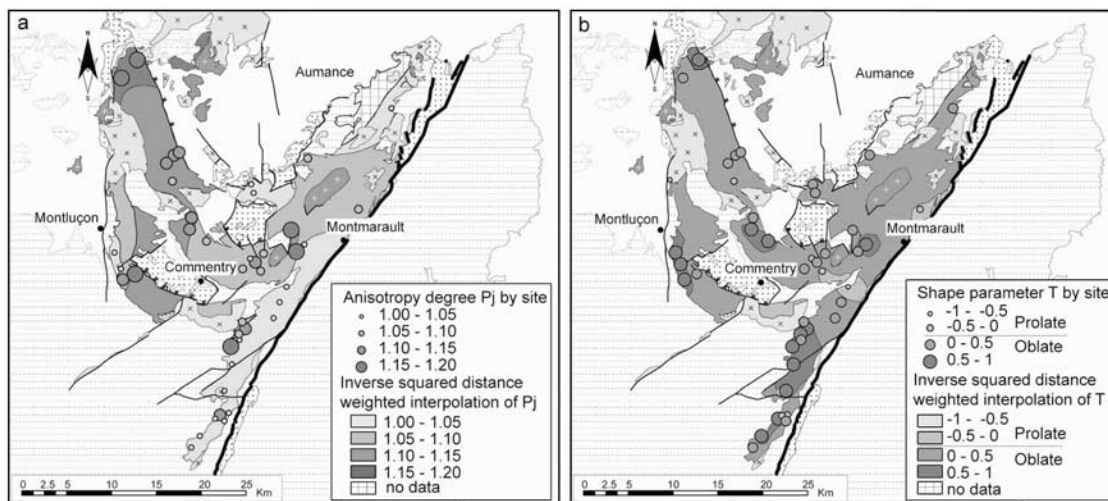
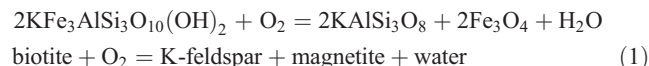


Figure 11. Geographic distribution of (a) the anisotropy degree P_j and (b) shape parameter T .

5. Discussion and Conclusions

[33] One difficulty in the study of pluton fabrics lies in measuring the planar and linear mineral preferred orientations, especially when the deformation is weak. AMS helps to better understand the mechanisms of pluton emplacement. Thus AMS analyses are applied here to the Montmarault pluton. Indeed, petrographic observations show that the Montmarault massif as a whole is characterized by a magmatic fabric and locally by a weak solid state fabric, as shown by both petrographic and AMS studies. The large range of spatial variations of the bulk magnetic susceptibility shown in this study and by the magnetic field intensity observed by previous airborne magnetic surveys (see part 2 of this study) argue for an important heterogeneous distribution of magnetic minerals at the pluton scale, which we attribute to the variation of magnetite concentration. In the western part of the pluton, the magnetic property is clearly controlled by the magnetite content in agreement with the positive anomaly of magnetic field intensity (Figure 3 in part 2), with high magnetic susceptibility (Figure 9) and well-identified magnetite (Figures 6, 8a, and 8b). However, paramagnetic minerals, such as biotite, are the main contributor to AMS measurements in the eastern part of pluton along the SHF with a negative magnetic anomaly (Figure 2 in part 2), lower magnetic susceptibility (Figure 9) and weak contribution of ferromagnetic minerals (Figures 6, 8c, and 8d). According to petrostructural study, *Sossa-Simawango* [1980] argued that magnetite and biotite crystallized contemporarily and that the magnetic heterogeneity might be due to the chemical zonation of the granitic pluton. Geochemical analyses show that the Montmarault massif is produced from a single magmatic chamber where silica and iron concentrations are heterogeneous (from 57% to 77% SiO_2 and from less than 1% to 7% Fe_{tot} on the whole rock [Sossa-Simawango, 1980]). This chemical zoning accounts for the formation conditions of the magnetite. To assess this mechanism, more petrological and chemical analyses are necessary all over the pluton. Moreover, the magma ascent may involve a high oxygen fugacity that may

in turn produce a significant modification of the chemical composition of ferromagnesian minerals, in particular for biotite [Frost and Lindsley, 1991; Gaillard *et al.*, 2001]. Indeed, the oxygen-dependent equilibrium between biotite and magnetite (equation (1)) indicates that an increase in the O_2 fugacity during the evolution of a magma system will displace this equilibrium to the right, consuming biotite and oxygen, as well as producing magnetite plus K-feldspar [Frost, 1990]:



From our own petrographic and rock magnetism studies, it may be concluded that biotite is the main contributor of the magnetic susceptibility in the eastern part of the pluton

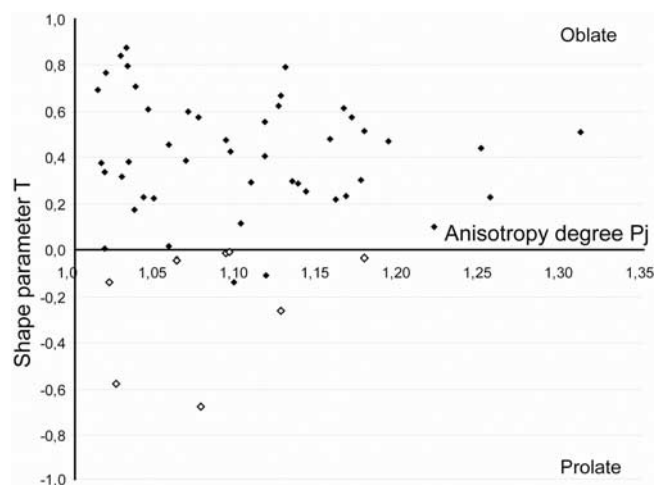


Figure 12. Plot of anisotropy degree P_j and shape T parameters showing dominant oblate AMS ellipsoid. Open and solid symbols indicate prolate and oblate shapes of AMS ellipsoid, respectively.

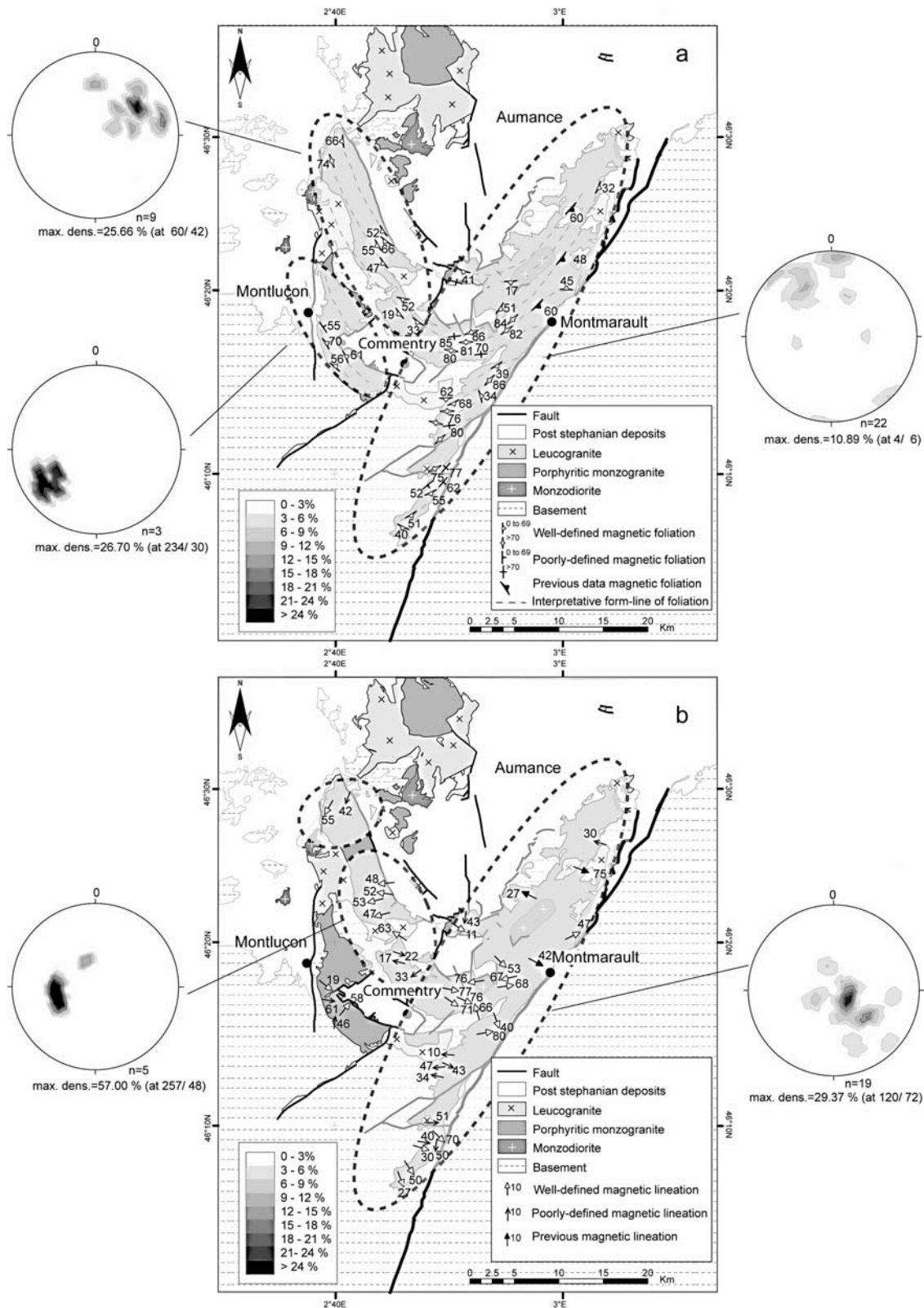


Figure 13. Magnetic foliation pole (K_3) and lineation (K_1) within the granitic pluton of Montmarault. Equal-area, lower hemisphere projection. Ellipses define areas with consistent AMS orientations. (a) Strike and dip of magnetic foliation at individual sites with the equal-area, lower hemisphere projection of poles to foliation of each area. (b) Plunge and trend of magnetic lineation at individual sites with the equal-area, lower hemisphere projection of lineation orientation of each area. Previous data come from *Sossa-Simawango et al.* [1987].

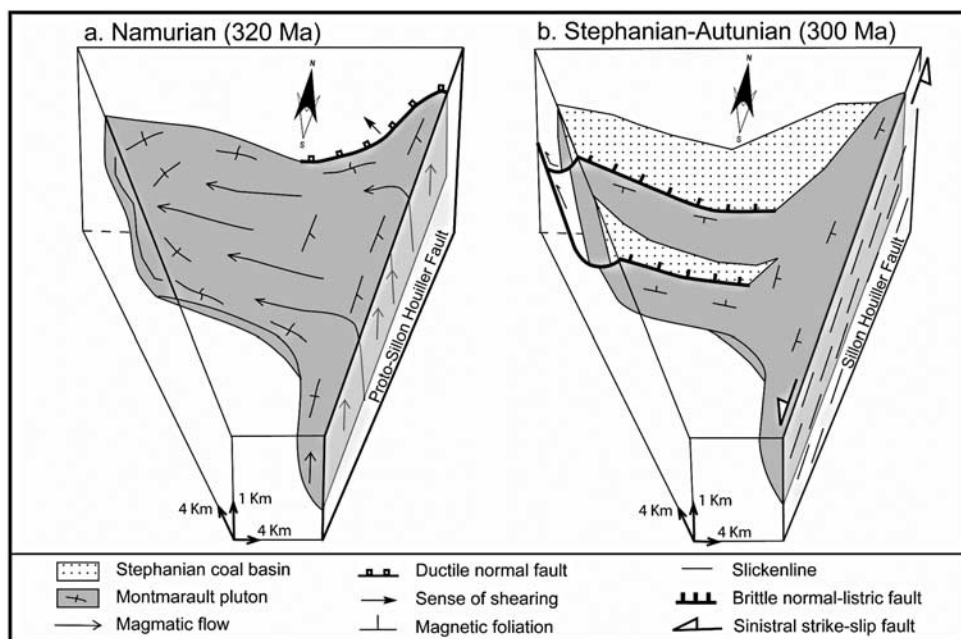


Figure 14. Emplacement model for the porphyritic Montmarault pluton. (a) Emplacement of the porphyritic granite during the Namurian NW-SE extensional tectonics through one feeder zone located along the SHF. (b) Opening of half graben basins filled by terrigenous and coal deposits during Late Carboniferous NE-SW extensional setting. The NE facing normal faults are responsible for the tilting to the southwest of the fault footwall (see text for further details).

along the SHF where the granitic massif is thicker, whereas the multidomain magnetite is the main contributor of the magnetic susceptibility in the western part where the massif is thinner (see following paragraphs and Figure 2 of part 2). As multidomain magnetite and biotite minerals carry normal magnetic fabrics [Rochette *et al.*, 1992], the AMS data may be directly used to infer their mineral fabrics. These fabrics could be interpreted as related to pluton emplacement and crystallization deformation because the microstructures are essentially of magmatic and locally weak solid-state deformation types.

[34] Sossa-Simawango *et al.* [1987] carried out a local AMS study in the northeastern part of the pluton that shows a good consistency of the fabric pattern with our observations (see black symbols in Figures 13a and 13b). Combining all data from these two studies allow us to draw the following conclusions. The magnetic fabric pattern is characterized by (1) oblate fabric dominance all over the pluton (Figures 11b and 12); (2) weaker anisotropy degree (P_1) along the SHF with respect to the western part of the pluton (Figure 11a); (3) high southeastward dip of the foliation and relatively high angle plunge lineation in the eastern part along the SHF; and (4) E–W trending lineation with “V” shape (SW and NE dipping) foliations in the western part of the massif (Figure 13a).

[35] The AMS results that mostly describe the magmatic fabrics of the Montmarault pluton during its emplacement can be highlighted when interpreted together with the gravity anomaly map (Figure 2 in part 2). Indeed, a well-defined negative gravity anomaly along the SHF is interpreted as the root zone of the pluton. This anomaly progressively vanishes northwestward suggesting that the

pluton spreads toward the northwest with a laccolite-like shape, in agreement with the relatively flat magnetic foliation (Figure 14a). The steep magnetic lineation in the pluton is perpendicular to the SHF and associated to a magnetic foliation strongly dipping toward the SHF. Moreover, a top-to-the-NW shearing develops along the NW margin of the pluton (Figures 14d and 14b). These geometric and kinematic features support the interpretation that, if the SHF existed at the time of pluton emplacement, i.e., in Namurian times, this fault that can be called the “Proto-Sillon Houiller Fault” would have acted as a feeder zone for the magma. However, the kinematics of the Proto-Sillon Houiller Fault remains hypothetical.

[36] The U-Th-Pb monazite age obtained in this study indicates that the Montmarault pluton was emplaced at circa 320 Ma. This age shows that the pluton is coeval with the Middle Carboniferous NW-SE extensional regime, already described in several Namurian granitic plutons in the French Massif Central (Figure 15). The Namurian to Westphalian (325–315 Ma), late orogenic NW-SE extension is conspicuously recorded by mineral and magnetic fabrics of leucogranites and granodiorites [Faure *et al.*, 1992; Faure, 1995; Talbot *et al.*, 2004, 2005; Be Mezème *et al.*, 2006b]. However, geochemical compositions of these granites are significantly different [Didier and Lameyre, 1971; Duthou *et al.*, 1984], indicating that they do not originate from the same magmatic sources. The consistency of the NW-SE trending lineation throughout the Namurian plutons of the French Massif Central [Gébelin *et al.*, 2004; Talbot *et al.*, 2004, 2005] indicates that these plutons emplaced into the metamorphic host rocks under the same tectonic regime within a relatively short time of circa 20 Ma. This NW-SE

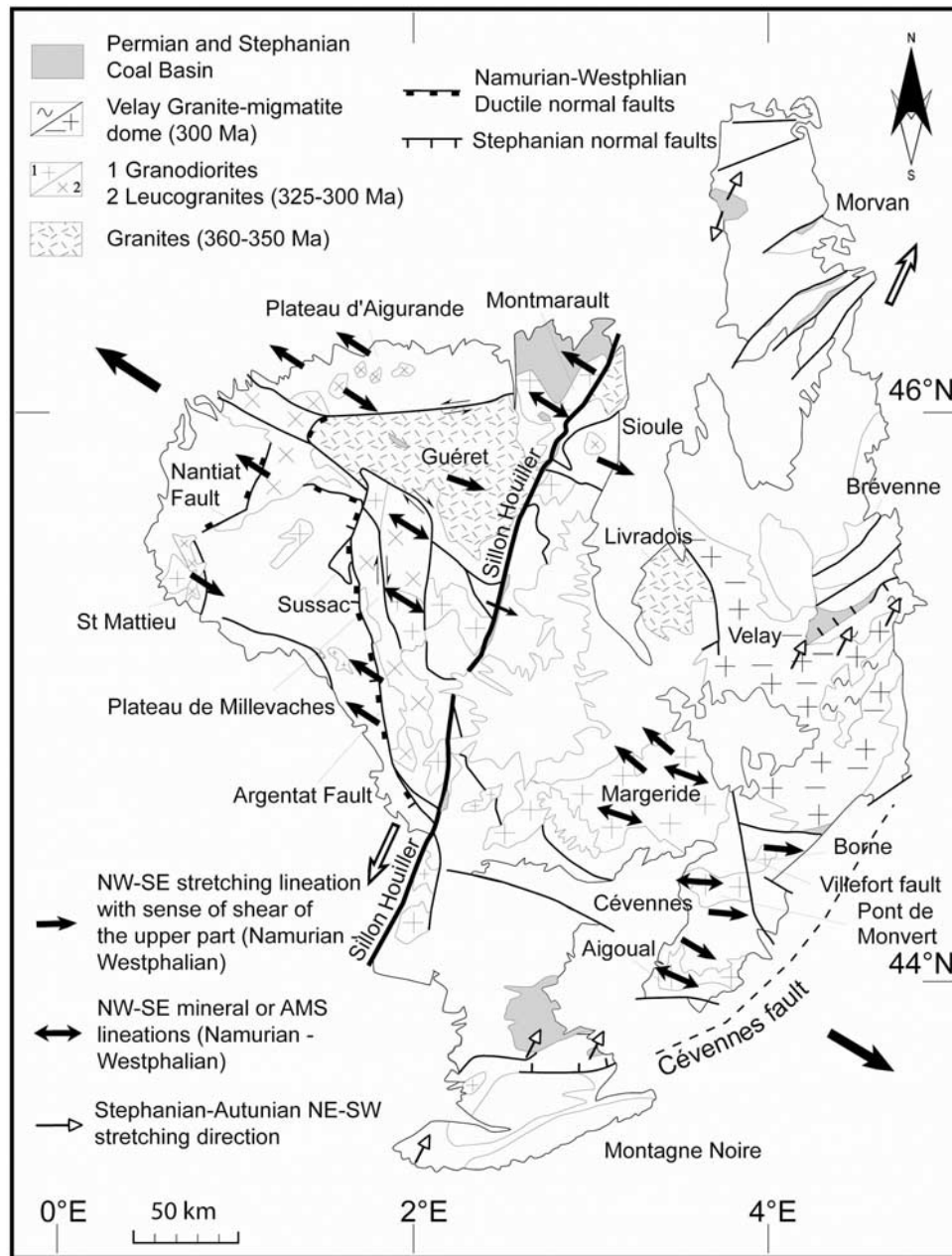


Figure 15. Tectonic map of the French Massif Central showing the two distinct Carboniferous extensional structures.

orientation of the stretching direction in the entire FMC is perpendicular to the Proto-Sillon Houiller Fault; therefore this structure probably behaved as an extensional structure.

[37] Furthermore, in an alternative hypothesis in which the Proto-Sillon Houiller Fault had acted as a left-lateral transfer fault during the emplacement of the Montmarault pluton, the mineral and AMS lineation would have trended parallel to the fault, i.e., in the NE-SW direction; and this direction is almost orthogonal to the NW-SE magnetic lineations we measured. In the present state of knowledge, as no field observation attest for ductile tectonics along the SHF, the existence of normal kinematics along the Proto-

Sillon Houiller Fault remains a working hypothesis to be confirmed by further studies.

[38] The present V shape of the foliation pattern of the Montmarault pluton is due to the postorogenic extensional tectonics developed around 300 Ma. The NE-SW Late Carboniferous extensional regime is recorded by the opening of intramountain Stephanian coal basins (e.g., Commentry and Montvicq) within the already crystallized Montmarault massif (Figure 1a). Indeed, our field observations show the existence of high-angle brittle fault which was already been interpreted as listric faults by *Faure* [1995]. The NW-SE trending and NE dipping listric normal faults are responsi-

ble for the southwestward tilting of the early magmatic foliation of the pluton (Figure 14b).

[39] According to the geochronological, structural and rock fabric investigations on the Montmarault granitic massif complemented by the geophysical data (part 2), the following conclusions can be drawn: (1) the Montmarault pluton formed in Middle Carboniferous (circa 320 Ma); (2) the syntectonic Montmarault pluton is rooted in its eastern part along the SHF and presents a laccolite-like shape in its western part; (3) its emplacement is controlled by NW-SE extensional tectonics which is consistent with the regional tectonic regime; (4) the SHF is interpreted as the feeding channel for the granitic magma emplacement during the Namurian-Westphalian period; (5) if the Proto-Sillon Houiller Fault was existed at circa 320 Ma, it probably acted as a normal fault; and (6) the final architecture of the pluton is due to the Late Carboniferous (circa 300 Ma) NE-SW extensional tectonics.

[40] **Acknowledgments.** This study was partially funded by “Référentiel Cartographique 3D intégré” project of Bureau de Recherche Géologique et Minière (BRGM). Constructive reviews by two reviewers are deeply acknowledged.

References

- Barbarin, B., J. M. Belin, A. Fernandez, J. Grolier, A. Lacour, and M. Turland (1985), Observations de pétrologie structurales sur le granite de Montmarault (Allier, Puy-de-Dôme), *Geol. Fr.*, 4, 381–388.
- Be Mezème, E., M. Faure, A. Cocherie, and Y. Chen (2005), In situ chemical dating of tectonothermal events in the French Variscan Belt, *Terra Nova*, 17, 420–426.
- Be Mezème, E., A. Cocherie, M. Faure, O. Legendre, and P. Rossi (2006a), Electron microprobe monazite geochronology of magmatic events: Examples from Variscan migmatites and granitoids, Massif Central, France, *Lithos*, 87(3–4), 276–288.
- Be Mezème, E., M. Faure, Y. Chen, A. Cocherie, and J.-Y. Talbot (2006b), Structural, AMS and geochronological study of a laccolith emplaced during Late Variscan orogenic extension: The Rocles pluton (SE French Massif Central), *Int. J. Earth Sci.*, 96(2), 215–228, doi:10.1007/s00531-006-0098-2.
- Berthier, F., J.-L. Duthou, and M. Roques (1979), Datation géochronologique Rb/Sr sur les roches totales du granite de Guéret (Massif Central). Age fini-dévonien de la mise en place de l'un de ses faciès, *Bull. BRGM*, 1(2), 59–72.
- Bingham, C. (1964), Distribution on a sphere and on the projective plane, Ph.D. thesis, Yale Univ., New Haven, Conn.
- Binon, M., and C. Pin (1989), Geochronologie Rb-Sr et U-Pb des granites du Mayet-de-Montagne et des Bois Noirs, Montagne bourbonnaise (Massif central), *Bull. Soc. Geol. Fr.*, 8, 695–703.
- Blès, J. L., D. Bonijoly, C. Castaing, and Y. Gros (1989), Successive post-Variscan stress fields in the French Massif Central and its borders (western European plate): Comparison with geodynamic data, *Tectonophysics*, 169, 79–111.
- Boissonas, J., and N. Debeglia (1976), Etude géophysique du granite magnétique de Montmarault (Allier) et corrélation avec la pétrographie, *Rapp. BRGM 76*, SGN 401 GPH.
- Bonijoly, D., and C. Castaing (1984), Fracturation et genèse des bassins Stéphaniens du Massif central français en régime compressif, *Ann. Soc. Geol. Nord*, 103, 187–199.
- Borradaile, G. J., and B. Henry (1997), Tectonic applications of magnetic susceptibility and its anisotropy, *Earth Sci. Rev.*, 42(1–2), 49–93.
- Bouchez, J. L. (1997), Granite is never isotropic: An introduction to AMS studies of granitic rocks, in *Granite: From Segregation of Melt to Emplacement Fabrics*, edited by J.-L. Bouchez, D. H. W. Hutton, and W. E. Stephens, pp. 95–112, Kluwer Acad., Dordrecht, Netherlands.
- Braun, I., J. M. Montel, and C. Nicollet (1998), Electron microprobe dating of monazites from high-grade gneisses and pegmatites of the Kerala Khondalite Belt, southern India, *Chem. Geol.*, 146, 65–85.
- Burg, J. P., J. P. Brun, and J. Van Den Driessche (1990), Le Sillon Houiller du Massif Central français: Faïlle de transfert pendant l'amincissement crustal de la chaîne varisque?, *C. R. Acad. Sci., Ser. II*, 311, 147–152.
- Cocherie, A., and F. Albarède (2001), An improved U–Th–Pb age calculation for electron microprobe dating of monazite, *Geochim. Cosmochim. Acta*, 65, 4509–4522.
- Cocherie, A., O. Legendre, J. J. Peucat, and A. N. Kouamelan (1998), Geochronology of polygenetic monazites constrained by in situ electron microprobe Th-U-total lead determination: Implications for lead behaviour in monazite, *Geochim. Cosmochim. Acta*, 62, 2475–2497.
- Cocherie, A., E. Be Mezème, O. Legendre, C. M. Fanning, M. Faure, and P. Rossi (2005), Electronmicroprobe dating as a tool for determining the closure of Th-U-Pb systems in migmatitic monazites, *Am. Mineral.*, 90, 607–618.
- Costa, S., and P. Rey (1995), Lower crustal rejuvenation and growth during post-thickening collapse from a crustal cross section through a Variscan core complex, *Geology*, 23, 905–908.
- Day, R., M. Fuller, and V. A. Schmidt (1977), Hysteresis properties of titanomagnetites: Grain-size and compositional dependence, *Phys. Earth Planet. Inter.*, 13, 260–267.
- Didier, J., and J. Lameyre (1971), Les roches granitiques du Massif Central français, in *Symposium J. Jung*, pp. 135–156, Géol., Géomorph. et Struct. Profondes du Massif Cent. Fr., Plein Air Serv., Clermont-Ferrand, France.
- Dumas, E., M. Faure, and J. Pons (1990), L'architecture des plutons leucogranitiques du plateau d'Aigurande et l'amincissement crustal tardi-varisque, *C. R. Acad. Sci., Ser. II*, 310, 1533–1539.
- Duthou, J. L., J. M. Cantagrel, J. Didier, and Y. Viallette (1984), Paleozoic granitoids from the French Massif Central: Age and origin studied by ⁸⁷Rb/⁸⁷Sr system, *Phys. Earth Planet. Inter.*, 35, 131–144.
- Ellwood, B. B., and D. B. Wenner (1981), Correlation of magnetic susceptibility with ¹⁸O:¹⁶O data in orogenic granites of southern Appalachian Piedmont, *Earth Planet. Sci. Lett.*, 59, 200–202.
- Faure, M. (1989), L'amincissement crustal de la chaîne varisque à partir de la déformation ductile des leucogranites du Limousin, *C. R. Acad. Sci., Ser. II*, 309, 1839–1845.
- Faure, M. (1995), Late Carboniferous extension in the Variscan French Massif Central, *Tectonics*, 14, 132–153.
- Faure, M., and J. Pons (1991), Crustal thinning recorded by the shape of the Namurian-Westphalian leucogranite in the Variscan belt of the northwest Massif Central, France, *Geology*, 19, 730–733.
- Faure, M., J. Pons, and J. F. Babinault (1992), Le pluton du Pont-de-Montvert: Un granite syntectonique extravasé vers l'Est pendant le désépaissement crustal varisque du Massif Central français, *C. R. Acad. Sci.*, 315, 201–208.
- Faure, M., E. Be Mezème, M. Duguet, C. Cartier, and J.-Y. Talbot (2005), Paleozoic tectonic evolution of Medio-Europa from the example of the French Massif Central and Massif Armoricaïn, *J. Virtual Explor.*, 19(5), 26 pp.
- Feybesse, J. L. (1981), Tectonique et microtectonique de la région de Laroquebrou (Cantal, Massif central français). Rôle de la déformation ductile et évolution du Sillon Houiller, Ph.D. thesis, 250 pp., Clermont Ferrand Univ., Clermont Ferrand, France.
- Frost, B. R. (1990), Biotite crystallisation as an oxidation agent in granitic rock, *Geol. Soc. Am. Abstr. Programs*, 22, A301.
- Frost, B. R., and H. Lindsley (1991), Occurrence of iron-titanium oxides in igneous rocks, in *Oxide Minerals, Rev. Mineral. Geochem.*, vol. 25, edited by D. H. Lindsley, pp. 433–468, Mineral. Soc. of Am., Washington, D. C.
- Gaillard, F., B. Scaillet, M. Pichavant, and J. L. Beny (2001), The effect of water and fO₂ on the ferric-ferrous ratio of silicic melts, *Chem. Geol.*, 174, 255–273.
- Gébelin, A., G. Martelet, M. Brunel, M. Faure, and P. Rossi (2004), Late Hercynian leucogranites modelling as deduced from new gravity data: The example of the Millevaches massif, Massif Central, France, *Bull. Soc. Geol. Fr.*, 175, 239–248.
- Grolier, J., and J. Letourneur (1968), L'évolution tectonique du grand Sillon Houiller du Massif Central français, paper presented at XXIII International Geological Congress, Int. Union of Geod. and Geophys., Florence, Italy.
- Hibbard, M. J. (1987), Deformation of incompletely crystallized magma systems: Granitic gneisses and their tectonic implications, *J. Geol.*, 95, 543–561.
- Hrouda, F. (1982), Magnetic anisotropy of rocks and its application in geology and geophysics, *Geophys. Surv.*, 5, 37–82.
- Jelinek, V. (1981), Characterization of the magnetic fabric of rocks, *Tectonophysics*, 79, 563–567.
- Joly, A., G. Martelet, Y. Chen, and M. Faure (2007), A multidisciplinary study of a syntectonic pluton close to a major lithospheric-scale fault—Relationships between the Montmarault granitic massif and the Sillon Houiller Fault in the Variscan French Massif Central: 2. Gravity, aeromagnetic investigations and three-dimensional geologic modeling, *J. Geophys. Res.*, doi:10.1029/2006JB004744, in press.
- Jover, O. (1986), Les massifs granitiques de Guéret et du nord-Millevaches. Analyse structurale et modèle de mise en place (Massif Central Français), Ph.D. thesis, 233 pp., Nantes Univ., Nantes, France.

- Ledru, P., J. M. Lardeaux, D. Santallier, A. Autran, J. M. Quenardel, J. P. Floc'h, G. Lerouge, N. Maillat, J. Marchand, and A. Ploquin (1989), Où sont les nappes dans le Massif Central français?, *Bull. Soc. Geol. Fr.*, *8*, 605–618.
- Ledru, P., G. Courrioux, C. Dallain, J. M. Lardeaux, J. M. Montel, O. Vanderhaeghe, and G. Vitel (2001), The Velay dome (French Massif Central): Melt generation and granite emplacement during orogenic evolution, *Tectonophysics*, *342*(3–4), 207–237.
- Letourneur, J. (1953), Le grand Sillon Houillier du plateau central français, *Bull. Carte Geol. Fr.*, *238*, 235 pp.
- Malavieille, J., P. Guihot, S. Costa, J. M. Lardeaux, and V. Gardian (1990), Collapse of the thickened Variscan crust in the French Massif central: Mont Pilat extensional shear zone and St-Etienne Late Carboniferous basin, *Tectonophysics*, *177*, 139–149.
- Matte, P. (1986), La chaîne varisque parmi les chaînes paléozoïques péri atlantiques, modèle d'évolution et position des grands blocs continentaux au Permo-Carbonifère, *Bull. Soc. Geol. Fr.*, *8*, 9–24.
- Menard, G., and P. Molnard (1988), Collapse of Hercynian Tibetan Plateau into a late Paleozoic European Basin and Range province, *Nature*, *334*, 235–237.
- Mollier, B., and J.-L. Bouchez (1982), Structuration magmatique du complexe granitique de Brême-St Sylvestre-St Goussaud (Limousin, Massif Central Français), *C. R. Acad. Sci., Ser. 2*, *294*, 1329–1334.
- Montel, J.-M., S. Foret, M. Veschambre, C. Nicollet, and A. Provost (1996), Electron microprobe dating of monazite, *Chem. Geol.*, *131*, 37–53.
- Montel, J.-M., J. Kornprobst, and D. Vielzeuf (2000), Preservation of old U-Th-Pb ages in shielded monazite: Example from Beni Bousera Hercynian Kinzigites (Morocco), *Journal of Metamorphic Geology*, *18*, 335–342.
- Parrish, R. R. (1990), U-Pb dating of monazite and its application to geological problems, *Can. J. Earth Sci.*, *27*, 1450.
- Paterson, S. R., R. H. Vernon, and O. T. Tobisch (1989), A review of criteria for the identification of magmatic and tectonic foliations in granitoids, *J. Struct. Geol.*, *11*, 349–363.
- Rochette, P., M. Jackson, and C. Aubourg (1992), Rock magnetism and the interpretation of anisotropy of magnetic susceptibility, *Geophysics*, *3*, 209–226.
- Sossa-Simawango, M. (1980), Contribution à la pétrologie, la géochimie, la géologie structurale du massif granitique de Montmarault (Massif Central français), Ph.D. thesis, Orléans Univ., Orléans, France.
- Sossa-Simawango, M., B. Henry, and L. Daly (1987), Magnetic structural analysis of the Montmarault granite (French Massif Central), *J. Struct. Geol.*, *9*, 911–914.
- Suzuki, K., and M. Adachi (1991), The chemical Th-U-total Pb isochron ages of zircon and monazite from the gray granite of the Hida terrane, Japan, *J. Earth Sci.*, *38*, 11–37.
- Talbot, J. Y., G. Martelet, G. Courrioux, Y. Chen, and M. Faure (2004), Emplacement in an extensional setting of the Mont Lozère-Borne granitic complex (SE France) inferred from comprehensive AMS, structural and gravity studies, *J. Struct. Geol.*, *26*, 11–28.
- Talbot, J. Y., M. Faure, Y. Chen, and G. Martelet (2005), Pull-apart emplacement of the Margeride granitic complex (French Massif Central): Implications for the late evolution of the Variscan orogen, *J. Struct. Geol.*, *27*, 1610–1629.
- Tauxe, L., T. A. T. Mullender, and T. Pick (1996), Potbellies, wasp-waists and superparamagnetism in magnetic hysteresis, *J. Geophys. Res.*, *101*, 571–583.
- Turland, M., R. Feys, F. Destieux, and D. Virlogeux (1989), Carte géologie France, scale 1:50,000, feuille Montluçon (619), Notice explicative par M. Turland, A. M. Hottin and R. Feys, 115 pp., Bur. de Rech. Géol. et Minière, Orléans, France.
- Turland, M., P. Gentilhomme, J. L. Duthou, D. D'Arcy, J.-P. Carroué, and N. Debeglia (1991), Carte géologie France, scale 1:50,000, feuille Montmarault (620), Notice explicative par M. Turland, P. Gentilhomme, J. L. Duthou, D. D'Arcy, J.-P. Carroué, and N. Debeglia, 114 pp., Bur. de Rech. Géol. et Minière, Orléans, France.
- Van den Driessche, J., and J. P. Brun (1989), Un modèle de l'extension paléozoïque supérieur dans le sud du Massif central, *C. R. Acad. Sci., Ser. 2*, *309*, 1607–1613.
- Vanderhaeghe, O., and C. Teyssier (2001), Partial melting and flow of orogen, *Tectonophysics*, *342*, 451–472.
- Vernon, R. H. (2000), Review of microstructural evidence of magmatic and solid-state flow, *Electron. Geosci.*, *5*, 2.
- Wendt, I., and C. Carl (1991), The statistical distribution of the mean squared weighted deviation, *Chem. Geol.*, *86*, 275–285.
- Williams, M. L., and M. J. Jercinovic (2002), Microprobe monazite geochronology: Putting absolute time into microstructural analysis, *J. Struct. Geol.*, *86*, 1013–1028.
- Zapletal, K. (1990), Low field susceptibility anisotropy of some biotite crystals, *Phys. Earth Planet. Inter.*, *63*, 85–97.

Y. Chen and M. Faure, Institut des Sciences de la Terre d'Orléans, UMR CNRS 6113, Université d'Orléans, BP 6759, F-45067 Orléans, France.

A. Joly and G. Martelet, Bureau de Recherches Géologiques et Minières, 3 avenue Claude Guillemin, BP6009, F-45060 Orléans Cedex 2, France. (aurore.joly@univ-orleans.fr)